Nano Research
2021, 14(6): 2003–2022
ISSN 1998-0124 CN 11-5974/O4
https://doi.org/10.1007/s12274-020-2955-x

Review Article

Transition metal dichalcogenide-based mixed-dimensional heterostructures for visible-light-driven photocatalysis: Dimensionality and interface engineering

Xiaorong Gan[1], Dangyuan Lei[2] (✉), Ruquan Ye[3], Huimin Zhao[4], and Kwok-Yin Wong[5]

[1] *Key Laboratory of Integrated Regulation and Resource Development on Shallow Lake of Ministry of Education, College of Environment, Hohai University, Nanjing 210098, China*
[2] *Department of Materials Science and Engineering, City University of Hong Kong, Hong Kong 999077, China*
[3] *Department of Chemistry, State Key Laboratory of Marine Pollution, City University of Hong Kong, Hong Kong 999077, China*
[4] *Key Laboratory of Industrial Ecology and Environmental Engineering (Ministry of Education, China) and School of Environmental Science and Technology, Dalian University of Technology, Dalian 116024, China*
[5] *Department of Applied Biology and Chemical Technology, The Hong Kong Polytechnic University, Hong Kong 999077, China*

Received: 23 April 2020 / **Revised**: 24 June 2020 / **Accepted**: 25 June 2020

ABSTRACT

Two-dimensional (2D) transition metal dichalcogenides (TMDCs) are emerging as promising building blocks of high-performance photocatalysts for visible-light-driven water splitting because of their unique physical, chemical, electronic, and optical properties. This review focuses on the fundamentals of 2D TMDC-based mixed-dimensional heterostructures and their unique properties as visible-light-driven photocatalysts from the perspective of dimensionality and interface engineering. First, we discuss the approaches and advantages of surface modification and functionalization of 2D TMDCs for photocatalytic water splitting under visible-light illumination. We then classify the strategies for improving the photocatalytic activity of 2D TMDCs via combination with various low-dimensional nanomaterials to form mixed-dimensional heterostructures. Further, we highlight recent advances in the use of these mixed-dimensional heterostructures as high-efficiency visible-light-driven photocatalysts, particularly focusing on synthesis routes, modification approaches, and physiochemical mechanisms for improving their photoactivity. Finally, we provide our perspectives on future opportunities and challenges in promoting real-world photocatalytic applications of 2D TMDC-based heterostructures.

KEYWORDS

two-dimensional semiconductors, transition metal dichalcogenides, mixed-dimensional heterostructures, solar photocatalysis, dimensionality and interface engineering

1 Introduction

Solar energy conversion and storage is a worldwide problem for the sustainable development of human society. Thus, global efforts have been made towards the development of renewable clean energy sources, to replace traditional fossil fuels [1–3]. Artificial photosynthetic systems are among the most promising of these strategies because solar energy is an abundant and easily available natural energy source [1, 4]. Hydrogen production through solar water splitting represents the ultimate goal in renewable energy research. Its efficiency depends on the rational design of stable, efficient, and low-cost photocatalysts with visible-light responsivity. In essence, the critical problem lies in understanding photo-induced charge kinetics, including charge generation under photoexcitation (solar-light absorption), charge transfer to a catalyst surface (charge separation/migration), and charge consumption for redox reactions [5–8].

Traditional bulk photocatalysts such as simple oxides (e.g., TiO_2), sulfides (e.g., CdS), complex oxides (e.g., Bi_2WO_6), and nitrides still exhibit low conversion efficiency in the visible-light range, mainly because of large bandgaps, low solar-light absorption, sluggish carrier mobility, and/or high carrier recombination rates [9]. It is well known that in addition to composition and atomic arrangement, dimensionality plays a critical role in determining the fundamental properties of these materials. Two-dimensional (2D) ultrathin nanomaterials are ideal candidates for constructing highly efficient photocatalysts because of their unique properties derived from quantum size and surface effects [10–16]. Because of their ultrathin planar structure and excellent optical properties, 2D nanomaterials are excellent substrates or co-catalysts for loading other nanoscale catalysts and improving photocatalytic activity [17–19]. Ultrathin planes can decrease the transfer distance of light-induced charges from the bulk to the surface for water-splitting reactions. Because of the large surface area of 2D nanomaterials, a large number of photons can be absorbed in a remarkably short time under a low photon-flux density [19, 20]. Furthermore, their planar structure allows more surface defects to appear because the atomic-escape energy becomes

Address correspondence to dangylei@cityu.edu.hk

relatively small. In general, such architecture has the benefit of permitting flexible modification or functionalization to further improve photocatalytic activity [15].

Among 2D nanomaterials, transition metal dichalcogenides (TMDCs) are able to complement or even surpass graphene (zero band gap) in electronic and optoelectronic applications because of their strong spin-orbit coupling and favorable electronic and mechanical properties. TMDCs possess a crystal structure consisting of an M layer sandwiched between two X layers, where M is a transition metallic element (M = Mo, W, V, Re, Ta, Ti), and X is a chalcogenide element (X = S, Se, Te). Structural phases of monolayer TMDCs contain mainly trigonal (1T, ABC stacking) and hexagonal (2H, ABA stacking) phases according to atomic arrangement or stacking order (Fig. 1(a)). In general, the 2H phase is thermodynamically stable, whereas the 1T phase is metastable. A 2H/1T phase transition can be realized via chemical (electron donation from intercalation species) or physical methods (e.g., strain effects) [21]. Their rich d electron configurations lead to various electronic structures of 2D TMDCs [22]. Depending on the composition and the number of layers, their electronic structures can exhibit features including those of a semiconductor (e.g., MoS_2, WS_2), semimetal (e.g., WTe_2, $TiSe_2$), metal (e.g., NbS_2, VSe_2), or superconductor (e.g., $NbSe_2$, TaS_2) [23, 24]. In addition, they can exhibit a direct-to-indirect bandgap transition when the thickness decreases. More importantly, their electronic and optoelectronic properties can be flexibly regulated via the layer stacking order, composition, and layer number/thickness without requiring stringent lattice matching. Compared with some traditional water-splitting photocatalysts, most 2D semiconducting TMDCs exhibit proper band gaps and can more efficiently convert solar energy [25, 26]. Experiments and density functional theory (DFT)-based first-principle calculations have demonstrated that 2D TMDCs are potential candidates for H_2 evolution reactions because the Gibbs free energy of adsorbed atomic hydrogen for TMDCs is close to zero (e.g., +0.08 V for the MoS_2 edge) [26, 27]. In light of these thickness-dependent properties, 2D TMDCs, especially some stable layered semiconductors (e.g., WS_2, WSe_2, MoS_2, $MoSe_2$, and $MoTe_2$), are suitable building blocks for constructing visible-light-driven photocatalysts (Fig. 1) [28, 29].

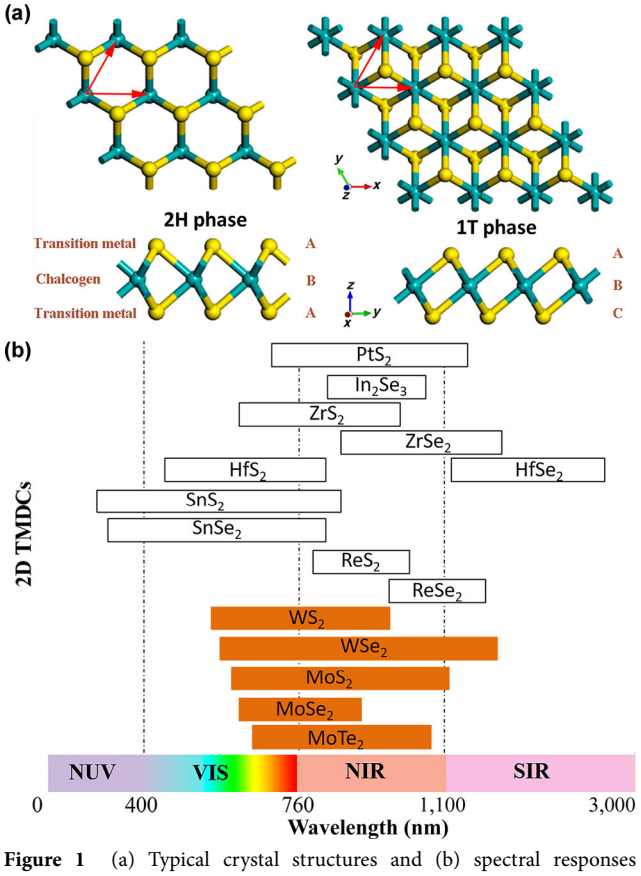

Figure 1 (a) Typical crystal structures and (b) spectral responses (depending on the number of layers) of 2D TMDCs (MX_2). Lattice vectors and stacking orders of atomic planes are indicated. NUV, VIS, NIR, and LIR represent near ultraviolet, visible, near infrared, and longwave infrared, respectively. The monolayers of 2D TMDCs labeled in orange are stable under ambient conditions (i.e. room temperature in air).

Similar to other 2D materials, pristine 2D TMDCs as photocatalysts still face some challenges related to their structure or properties because of easy restacking, sluggish charge dynamics, and/or poor visible-light harvesting or conversion. In addition, they face compromises in some related factors, such as light absorption range versus redox potentials, and active site versus conductivity. Therefore, it is necessary to modify or functionalize 2D TMDCs. Fortunately, 2D TMDCs offer a promising platform that allows creation of heterostructures with a variety of properties. In addition, the surface functionalization of 2D TMDCs is flexible and readily performed under mild conditions, without pretreatments by the strong acids or dangerous oxidizing agents that are usually used for the modification of graphene [30–34]. In addition to the planar edges of 2D TMDCs, their inert basal planes can also be (covalently) functionalized via liquid-phase exfoliation (LPE) or direct mixing with some solvents. The principles of surface functionalization comply with "click" reaction or Lewis acid–base chemistry [32, 34, 35]. Compared with pristine 2D TMDCs, 2D TMDC-based heterostructures formed via surface or interface functionalization can better meet the demands of high-performance photocatalysts. They have received widespread attention for photocatalytic applications because of their exceptional properties including, but not limited to, a sufficient potential to achieve overall water splitting, a narrow band gap to harvest more visible photons, and good stability against photo-corrosion.

The past decade has witnessed the successful development of 2D TMDCs in photocatalysis. Although several articles have reviewed strategies for surface functionalization and interface modulation of 2D TMDCs at the atomic or molecular level for various energy applications [5, 25–27, 36–39], a comprehensive overview on the recent remarkable progress in 2D TMDCs for visible-light-driven photocatalysis, especially for application in high-efficiency solar water splitting through regulation of the dimensionality and interface of 2D TMDC-based heterostructures, is still lacking. To fill this gap, the present review focuses on constructing 2D TMDC-based mixed-dimensional heterostructures, including mainly zero-dimensional (0D)–2D, one-dimensional (1D)–2D, and 2D–2D systems, and some complex three-dimensional(3D) hierarchical hybrid structures, which are also divided into the aforementioned types. First, we outline developments in 2D TMDCs and their pros and cons as building blocks of semiconductor photocatalysts for solar water splitting. Next, we discuss in detail the physiochemical mechanisms, varieties, and advantages of 2D TMDC-based heterostructures as visible-light-driven photocatalysts for water splitting from the perspective of energy band alignment. Note that we have avoided elaborating the physical and chemical properties and synthesis methods of pristine 2D TMDCs and their nanocomposites because several representative review articles have already documented these aspects [40–43]. Instead, we summarize the applications of mixed-dimensional heterostructures in photocatalytic water splitting under visible-light irradiation, and we especially

highlight the synthesis methods and modification approaches used for improving the photoactivity of 2D TMDCs. Finally, we provide our opinion on the future development and challenges of 2D TMDC-based heterostructures. Because of a dramatic increase in studies and publications in this active field, this review may not be able to include all relevant results that have been published in the past.

2 Principle of 2D TMDC-based photocatalytic water splitting

Photocatalytic water splitting is performed via energy transition from solar power to chemical energy with a large positive change of $\Delta G° = 237$ kJ/mol for the Gibbs free energy [44, 45]. Ideal photocatalysts should possess proper electron energy structures for strong photo-absorption over a wide range of the solar spectrum. Moreover, they should have high charge mobility, suitable Fermi levels, high stability, and robust photo-corrosion resistance for maximum solar-light conversion efficiency [46]. For higher quantum efficiency, improving the solar-light absorption is necessary, which can be tuned via control over the doping density, defect levels, local excitonic effects, and structural responses. Furthermore, the adsorption of light can be modified by the environment or by external fields, such as electric fields, optical fields, magnetic fields, temperature, and pressure, which can be correspondingly classified into all-optical, electro-optic, thermo-optic, magneto-optic, acousto-optic, and mechano-optical modulators [47]. Despite being atomically thin, many 2H-phase TMDCs can interact strongly with visible light in the solar spectrum (Fig. 1(b)). The interaction between light and 2D TMDCs can be described using the absorption coefficient ($\alpha(h\nu)$),

$$\alpha(h\nu) \propto \sum P_{12} g_V(E_1) g_C(E_2) \quad (1)$$

Equation (1) implies that light adsorption is related to the excitation probability (P_{12}) of an electron from its initial state, E_1, to its final state, E_2, and the electron densities, $g_V(E_1)$ and $g_C(E_2)$, in the two states. A monolayer MoS_2 can absorb approximately 10% of vertically incident light at excitonic resonances (615 and 660 nm) because of its direct bandgap structure. Furthermore, its total absorption can be further improved via combination with other layered nanomaterials to form van der Waals (vdW) heterostructures [48]. In addition to light adsorption, other properties, such as carrier concentration, mobility, and optical bandgap are readily regulated through the influence of the substrates around them [49, 50]. For example, plasmon–phonon coupling between 2D materials and polar substrates forms new mixed states such as plasmon–phonon–polaritons [10]. As such, interface engineering is frequently used to optimize the light absorption and behavior of charge carriers in 2D TMDCs [25].

The band gap energy (E_g) of a photocatalyst determines the light absorption range, whereas the positions of conduction band (CB) and valence band (VB) edges together determine the redox potentials [51]. Proper photocatalysts should possess E_g >1.23 eV (i.e., edge wavelength of absorption λ < 1,000 nm). For an effective visible-light-driven photocatalyst, when the light absorption and the redox potentials of charges are considered, a band gap of 1.23–3 eV is needed [25]. The band structure is just a thermodynamic requirement, whereas other factors such as overpotential, charge separation, mobility, and lifetime will strongly affect photoactivity [45, 51].

Water splitting using pure 2D semiconductors is involved in a first-step photoexcitation system. It faces a series of challenges in balancing several factors, such as VB/CB levels, light-harvesting capability, electron–hole separation efficiency, and surface reaction rate. In the charge transfer process via one-step photoexcitation in photocatalysts, heavy recombination occurs between electrons and holes via strong Coulomb forces. Consequently, a small portion of the remaining charges can participate in water splitting at the catalyst–electrolyte interface with certain catalytic active sites [52]. These active sites stem from structural defects located at low-coordinated sites, such as edges, terraces, kinks, and/or corner atoms [5, 21, 53]. Currently, most photocatalysts hardly realize overall water splitting, and each half reaction requires the addition of sacrificial reagents. Compared with H_2 evolution, the release of diatomic O_2 is challenging because there are four electrons and four protons involved in the eventual formation of an O–O bond. The alternative pathway is based on a stepwise two-electron/two-electron process ($2H_2O \rightarrow H_2 + H_2O_2$; $2H_2O_2 \rightarrow 2H_2O + O_2$). This route may be a viable and effective approach because the second step is exothermic ($\Delta G = 106.1$ kJ/mol), requiring an overpotential lower than in an endothermic process.

Pristine 2D TMDCs as photocatalysts possess fewer electrons or holes available for photochemical reactions and exhibit significantly faster kinetics (10–100 ns) for charge recombination, compared with hybrid photocatalysts (100 ns–several ms) [54]. Furthermore, some contradictions cannot be easily overcome by pristine 2D TMDCs, even after simple functionalization, such as elemental doping [55]. For example, narrow-bandgap semiconductors are more likely to harvest visible light (43% of solar spectrum) but lead to a high probability of recombination of photo-generated electron–hole pairs. In addition, the energy positions of their band edges are frequently incompatible with the redox potentials of H_2O [56]. By contrast, hybrid heterostructures, as photocatalysts composed of multiple integrated functional components with different dimensionalities, can make full use of the advantages of each component while overcoming their drawbacks at the same time [57]. Therefore, hybrid photocatalysts can meet various rigid demands, which may include increasing light absorption, promoting separation and transportation of charge, enhancing redox catalytic activity, and prolonging functional life-time [58, 59].

One of the preconditions for constructing effective 2D TMDC-based heterostructures is proper energy alignment between the co-catalysts and main catalysts or between the main catalysts. This is called energy band engineering, which opens up promising routes toward the flexible design and optimization of electronic and optoelectronic properties [60]. Based on the type of majority charge carriers in semiconductors, 2D TMDCs can be divided into p-type semiconductors and n-type semiconductors. The p–n heterojunctions are viewed as the most challenging yet effective photocatalytic materials [61] because their special structure can generate a space charge region, which stems from the depletion of electrons from the n-type semiconductor and holes from the p-type semiconductor near that region. The space charge region generates an electrostatic field that can facilitate the transport of electrons and retards the recombination of photo-generated electron–hole pairs [62]. From the point of view of energy band alignment, 2D TMDC-based heterostructures can be classified into Z-scheme systems, Schottky junction systems, type I heterostructure systems with a straddling gap, and type II heterostructure systems with a staggered gap (Fig. 2). Type II semiconductor heterostructures are beneficial for the formation of an indirect exciton, where the electron is located in one 2D material and the hole in another 2D material [63]. On the other hand, compared with type II and other types, Z-scheme systems can mimic a natural photosynthesis system. Photocatalysts

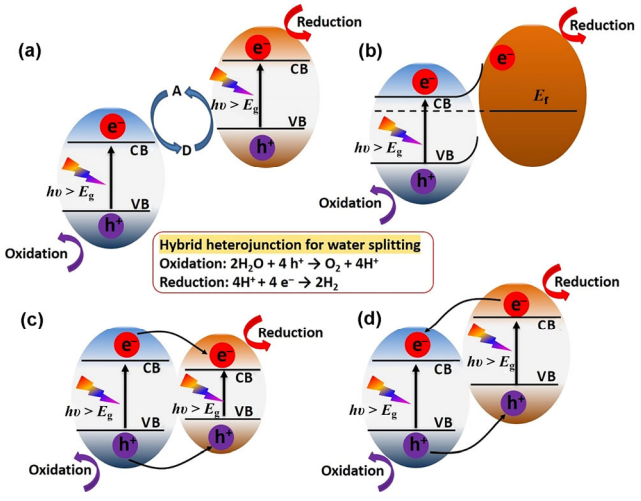

Figure 2 Schematic energy diagrams for Z-scheme system (a), Schottky junction (b), type I heterostructure (c), and type II heterostructure (d). CB, conduction band; VB, valence band; E_g, band gap; E_f, Fermi level. D and A indicate electron donating and accepting species, respectively.

based on a Z-scheme system can increase light harvesting and can have spatially separated reductive and oxidative active sites and well-preserved strong redox abilities [64, 65]. By contrast, other types of heterostructures compensate for the spatial separation of carriers via a decrease in redox abilities.

3 Strategies for constructing 2D TMDC-based heterostructures

The critical task in the construction of proper heterogeneous photocatalysts is determining and implementing a way of effectively regulating the thermodynamic and kinetic processes of photo-generated charges. General strategies include structural defects (e.g., S vacancies), doping, adsorbed organic molecules for sensitization, and hetero-combination with other low-dimensional nanomaterials, which are involved in energy band engineering and morphology or interface engineering (Fig. 3).

These strategies are performed in an attempt to obtain a better balance between related factors affecting photocatalytic activity. For example, the active sites of 2D nanomaterials stem

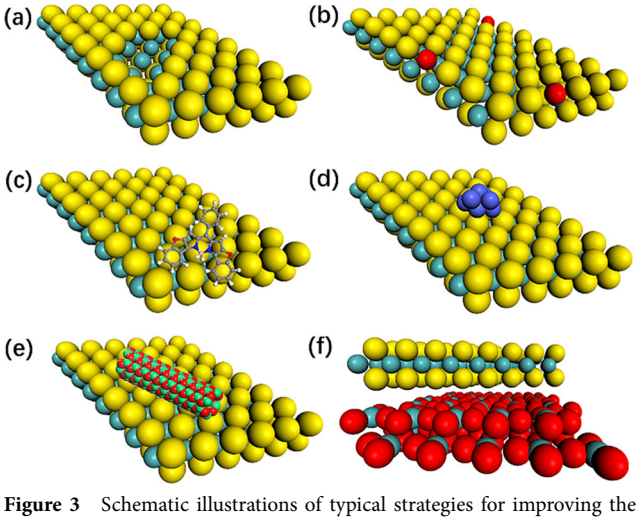

Figure 3 Schematic illustrations of typical strategies for improving the photoactivity of pristine 2D TMDCs by (a) defects engineering, (b) heteroatoms doping, (c) organic molecules adsorption, and hetero-combination with (d) 0D, (e) 1D, and (f) 2D nanomaterials. Taking the surface functionalization of 2D MoS_2 as an example, cyan, yellow, red, gray, blue, white, pink, dark blue, and green balls represent the Mo, S, O, C, N, H, P, Pt, and Ti atoms.

from structural disorders such as dislocations and vacancies, while they can lead to electron scattering and combination between electrons and holes. Simple surface modifications can hardly lead to the construction of ideal photocatalysts (Figs. 3(a)–3(c)), even though they do improve to some extent the photoactivity of pristine 2D TMDCs. For example, introducing dopants (e.g., cobalt and nickel ions) into a MoS_2 framework can improve the catalytic activity of basal planes by increasing the density of unsaturated atom sites or other structural defects. These methods adjust the CB and band gap and enhance the water reduction reaction and conductivity. However, it is difficult to subtly regulate the position of the VB for O_2 evolution [66]. Similarly, organic dyes as sensitizers mainly provide additional light-harvesting capability via a push-pull effect between the donor and acceptor, and improve the chemical stability of 2D TMDCs [67]. However, organic dyes easily suffer from degradation and adjust the redox potentials of 2D TMDCs only slightly towards satisfactory performance [68].

Moreover, conventional sensitized dyes need to be regenerated by electron-donor agents (e.g., ethylenediaminetetraacetic acid or triethanolamine) to close the catalytic cycle. For example, compared with MoS_2 modified by organic molecular dye sensitizers, dye molecules-MoS_2-graphene and dye molecules-MoS_2-g-C_3N_4 (g-C_3N_4 = graphitic carbon nitride) exhibit better visible-light activity for photocatalytic water splitting [67, 68]. In a previous review article, we systemically summarized the strategies for regulating structure–property relationships based on elemental doping, creation of defects (e.g., vacancies) or specific facets, and combination with dyes as sensitizers for visible-light-driven photocatalytic water splitting [5]. However, given their intrinsic limitation, the following discussions are focused mainly on 2D TMDC-based mixed-dimensional heterostructures, specifically on 0D–2D, 1D–2D, and 2D–2D heterostructures (Figs. 3(d)–3(f)). Such 2D TMDC-based heterogeneous photocatalysts incorporate a separate light absorber material and a co-catalyst [69], providing more possibilities for effectively regulating photoactivity and other measures of performance. Based on the materials involved, heterogeneous photocatalysts can be divided primarily into semiconductor–co-catalyst heterostructures, semiconductor–metal heterostructures, semiconductor–semiconductor heterostructures, and semiconductor–non-metal heterostructures [69–72].

3.1 0D–2D nano-heterostructures

In heterostructures, 0D nanomaterials are usually used as co-catalysts. They can promote charge separation by accepting electrons or holes from light-harvesting 2D TMDCs. In addition, they can provide more active sites for reduction or oxidation reactions, enhance overall stability, reduce activation energy for surface chemical reactions, and suppress side or back reactions [73–75]. In addition to the component and dimensionality/microstructure (e.g., core/shell), size effects of co- catalysts, from nanoparticles to single atoms, can flexibly regulate photoactivity [76–78], mainly because the electronic properties, structural stability, and exciton generation of 0D semiconductors are dependent on their size, shape, and composition when subjected to photoexcitation. For example, when their size is smaller than the Bohr radius (e.g., ~ 18 nm for PbS, ~ 46 nm for PbSe, and ~ 5 nm for CdSe), they can harvest light energy in the visible and infrared regions of solar light [78].

0D–2D hybrid systems can create synergies in photo-catalytic activity. Typically, 0D metal nanoparticles as co-catalysts can enhance the absorption of nearby 2D TMDCs through two potential types of mechanisms. The first type is a dipolar oscillation of all electrons in the metallic nanostructure, which

induces strong absorption of electromagnetic energy because 0D metallic nanostructures can act as plasmonic antennas for efficient light harvesting and concentration [79]. The other type is surface plasmon resonance (SPR) of 0D metal nanomaterials, which can greatly enhance the local optical field, especially in gap regions between the 0D metal nanomaterials [80]. As a result, the SPR of the 0D metal nanomaterials (e.g., nanoparticles) enhances the light absorption and photocatalytic activity of 2D TMDCs as supporting materials [81]. In addition, 0D–2D hybrid systems can enhance charge separation by transferring photo-excited electrons from metal nanoparticles to the CB of 2D TMDCs via the formation of a Schottky junction [82]. Carriers formed by surface plasmon polaritons (SPPs) possess lower energies than those by SPR, and have a low probability of crossing the potential interface barrier [83].

In a 0D–2D hybrid system, metal nanoparticles act as electron sinks and as conductive "wires" for accelerating electron transfer or charge separation. Electrons can be injected into the CB of 2D TMDCs. The process is quite important for wide-bandgap semiconductors, which can improve the redox abilities of photo-generated charges because, to some extent, this process overcomes the limitation of energy alignment. 2D TMDCs may promote electron–hole separation, provide active sites, and act as substrates for suppressing the aggregation of 0D nanoparticles [84, 85]. However, in some cases, metal nanomaterials as co-catalysts can catalyze the recombination of H_2 and O_2 into water, leading to a loss in overall efficiency. Therefore, it is necessary to add effective recombination-blocking materials, such as acid-tolerant SiO_2, MoO_x, or CrO_x, to prevent the facile reverse reaction [86–88]. In general, the combination of 0D nanomaterials and 2D TMDCs can allow flexible tuning of charge transfer at their interfaces. Consequently, this combination provides additional active sites for photochemical reactions to decrease overpotential. Moreover, these hybrid materials can better realize energy level matching between donor and acceptor materials, and use solar energy in a more effective way [78].

3.2 1D–2D nano-heterostructure

1D nanostructures have the smallest dimension for efficient transport of electrons and optical excitation because they have a long axis for the absorption of incident sunlight but a short radial distance for the separation of photo-generated charge carriers [89, 90]. Compared with 0D nanoparticles, 1D or 2D nanostructures generally have higher mobility and lower charge-recombination rates [91]. Because of their large length-to-diameter ratios, 1D nanomaterials can be more easily separated and recycled after finishing photoreactions. 1D–2D heterostructures can fully integrate the merits, and mitigate the drawbacks, of the single units, such as the low surface area of 1D nanowires and the restacking of 2D nanosheets. They may enable novel functions, which are not available to each of the components [89, 92]. Highly conductive 1D nanomaterials, such as carbon nanotubes and carbon nanofibers, can be used as electron shuttle mediators or excellent electron acceptors, to improve electron transfer and decrease the recombination rate of charge carriers [93]. 1D nanomaterials with mesoporous architectures possess large surface areas and expose adequate active sites. Thus, such materials are good candidates for the construction of 1D–2D hybrid photocatalysts [94, 95].

3.3 2D–2D nano-heterostructure

A plethora of opportunities become available when several 2D crystals are held together in one vertical stack by vdW forces because they allow a far greater number of combinations than any traditional growth method. For example, the growth of 2D–2D heterostructures is flexible without the requirements of lattice matching and processing compatibility. The vdW gaps in 2D–2D heterostructures can be treated as 2D nanoscale spacing that can change the microenvironment of active sites via confinement effects (i.e., geometric constraint and confinement field). Consequently, catalytic reactions in such confined spaces exhibit faster kinetics than in an open system [96, 97].

For hetero-photocatalysts, the interface is the most important factor in determining performance [98]. Compared with 0D–2D and 1D–2D heterostructures, 2D–2D hybrid systems exhibit better coupled interfaces, which can significantly improve photoactivity. The formation of an intimate interface between two types of 2D nanomaterials favors exciton dissociation due to the formation of a built-in potential, thus improving the photocatalytic quantum efficiency. Intimate interfaces can occur between 2D nanomaterials, even when they suffer from a lattice mismatch. The large contact areas in 2D–2D vdW heterostructures can better promote the transfer and separation of electron–hole pairs. In addition, their redox potentials can be readily regulated to match the overall water splitting reactions via the integration of a hydrogen evolution photocatalyst and/or an oxygen evolution photocatalyst in a flexible way. 2D–2D heterostructures are beneficial for the improvement of stability because of the alleviation of photocorrosion and agglomeration.

4 Applications in visible-light-driven water splitting

As mentioned before, pristine 2D TMDCs as photocatalysts do not easily meet the stringent demands of ideal photocatalysts, for example, there is a need for better balance between the wide light absorption range and the high redox potentials [59, 99, 100]. The plane edges and point defects in TMDCs easily suffer from significant photocorrosion, and some single-layer TMDCs are unstable even at room temperature [101]. For example, single-layered titanium sulfide (TiS_2) nanodisks can be oxidized by water and oxygen to form titanium oxide [102]. Moreover, research studies have shown that photocatalytic stability is anisotropic for exfoliated single- and few-layer MoS_2 immersed in water [101, 102]. Thus, the basal plane of MoS_2 is stable under photocatalytic conditions, but the edge sites are highly affected by photoinduced corrosion processes. In addition, pristine 2D TMDCs undergo substantial charge recombination on the surface because of a lack of sufficient driving force for separating photo-generated charge carriers [59, 100, 103]. In contrast, engineering heterostructures via the combination of 2D TMDCs and low-dimensional nanomaterials is more effective for improving stability and photocatalytic performance [26, 38, 104]. For example, MoS_2 nanosheets can be modified using Ag_3PO_4 and TiO_2 to form 3D hierarchical semiconductor composites, which exhibit better anti-photocorrosion than pure MoS_2 nanosheets [57]. 2D TMDCs as cocatalysts can also improve the photostability of other catalysts through the timely consumption of photo-generated charges, particularly holes. A hybrid photocatalyst composed of WS_2 nanosheets and CdS nanoparticles exhibits better photostability and photoactivity than those of pure CdS nanoparticles [28]. Therefore, generally, hybrid heterostructures can better suppress charge recombination, facilitate charge separation, provide additional photovoltage to drive the surface

reaction, and suppress the photocorrosion of semiconductors via efficient charge extraction. Next, we will highlight mixed-dimensional heterostructures based on 2D TMDCs and other low-dimensional nanomaterials.

4.1 0D–2D hybrid heterostructures for water splitting

Different size/shape tunable plasmonic noble metals and semiconducting nanomaterials remain as the leading inorganic catalytic materials. Based on the principle of excitation and charge transfer, metal–semiconductor hybrid photocatalysts can be broadly divided in two categories: 1) either metal or semiconductor is photoactive, or 2) both of them are photo-sensitized and absorb solar light. Generally, 0D–2D hybrid heterostructures belong to the latter group, mainly because of the narrow band gap of 2D TMDCs.

For 2D TMDCs, active sites or facets with higher surface energies are not only beneficial for chemical adsorption and dissociation of water but also enhance electron scattering because these active sites usually stem from structural disorders or structural defects [105]. The crystal defects in the bulk part of the material can accelerate the recombination rate of photo-generated electron–hole pairs. Such a challenge can be overcome via the combination of 0D nanomaterials and 2D TMDCs to form nano-heterostructures [106]. The catalytic activity of 0D nanomaterials strongly depends on preparation methods and support materials (Table 1). For example, their crystalline facets with high work functions can accumulate photo-excited electrons via spatial separation owing to their varying charge density [107]. It should be noted that not all 2D nanomaterials can offer an appropriate work function for combining with 0D nanomaterials to form nanoscale heterostructures.

In 0D–2D hybrid heterostructures, the 0D nanomaterials may be transition metals, noble metals, transition metal oxides, and/or transition-metal sulfides (Table 1). They usually, but not always, act as co-catalysts for providing sites for water oxidation and/or reduction, and preventing the combination of electrons and holes [63]. 0D metal compounds with d^0 ions (Ti, Zr, Nb, and Ta) and d^{10} ions (Ga, In, Ge, Sn, and Sb) exhibit activities involved in the overall water splitting reaction [108]. 0D noble metal nanoparticles can act as visible light absorbers and thermal redox active centers because of local surface plasmon resonance (LSPR), which can significantly improve overall photoconversion efficiency via direct electron transfer, local electromagnetic field enhancement, or resonant energy transfer [109–111]. Generally, LSPR includes many plasmon modes, such as dipole plasmon mode, quadrupole mode, and considerably higher plasmon modes. For photocatalytic applications, LSPR refers primarily to the dipole plasmon mode (Fig. 4), which arises from collective in-phase oscillations of the free electrons of metals with the incoming electric field. This phenomenon is dependent on the size, shape, and environment of 0D noble-metal nanoparticles and is used to improve the absorption of low-energy photons and form plasmonic "hot electron" injection without changing the bandgaps of the semiconductors.

Two or more noble metal nanostructures can lead to an SPR-coupling effect, which can greatly enhance the localized electromagnetic field. In general, the SPR effect of Au or Ag nanoparticles (NPs) leads to a higher absorptivity of visible light and enhances the conversion of resonant photons in the visible-light region into energetic electrons. The results are ascribed to charge redistribution, which shifts the Fermi level of 2D semiconductors as substrates. Different from Au or Ag NPs, Pt NPs with a larger work function can absorb scattered light in the near-field of the dielectric surfaces of the support materials and boost the formation of electron–hole pairs [112]. In return, the 2D TMDCs provide the 0D nanoparticles with a local dielectric environment that strongly affects their plasmonic near-field and consequently regulates photocatalytic activity. For

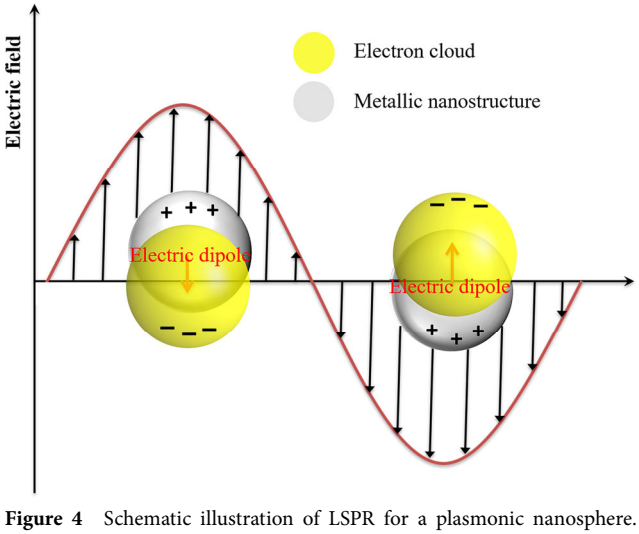

Figure 4 Schematic illustration of LSPR for a plasmonic nanosphere. LSPR represents localized surface plasmon resonance.

Table 1 Typical 0D–2D hybrid heterostructures as visible-light-driven photocatalysts for water splitting

Sample	Main synthesis methods	Roles of 2D TMDCs	Light source	H_2 (mmol/(g·h))	Ref.
Au multimer@MoS_2	Seed-mediated and hydrothermal methods	Main catalyst for exciton generation	300 W Xe lamp (λ = 530 or λ = 630 nm)	0.4 or 1.04	[113]
Monolayer WS_2-CdS	Wet-chemical method	Active sites	300 W Xe lamp (λ > 420 nm)	1.98	[119]
Monolayer MoS_2-CdS	Wet-chemical method	Active sites	300 W Xe lamp (λ > 420 nm)	1.47	[119]
WS_2/CdS	Impregnation and calcine	Cocatalyst	300 W Xe lamp (λ > 420 nm)	0.2	[162]
Cr NP–MoS_2 NS	A solution-based method	Decoupling light absorption	300 W Xe lamp (λ > 420 nm)	38	[123]
Ag NP–MoS_2 NS	A solution-based method	Decoupling light absorption	300 W Xe lamp (λ > 420 nm)	107	[123]
CdS@MoS_2	Hydrothermal method	Reducing energy barrier, active sites	300 W Xe lamp ($\lambda \geq$ 420 nm)	1.72	[134]
MoS_2/black TiO_2	Solid-state chemical reduction, calcination	Active sites	300 W Xe lamp (λ > 420 nm)	0.56	[163]
MoS_2/Mo_2C/CdS	Hydrothermal method	Active sites	300 W Xe lamp (λ > 420 nm)	34	[164]
WS_2/$ZnIn_2S_4$	Liquid exfoliation route and post-annealing process	Cocatalyst, active sites	300 W Xe lamp (λ > 420 nm)	2.55	[165]

example, under the same excitation light, the strength of the near-field gradually increases from Au monomer to dimer, and then to oligomer, because the in-phase couplings of Au oligomer produce a stronger near-field enhancement (Fig. 5(a)). More light energy can be stored in the inter-particle gaps at long wavelength (630 nm) than at short-wavelength (325 nm) because of the LSPR peak of the Au NPs. Furthermore, the highest photocurrent (under light illumination at a wavelength of 325 nm) can be obtained in Au multimer@MoS_2 samples because of better electron–hole separation performance (Fig. 5(b)). Similarly, under illumination of light with a wavelength of 530 or 630 nm, Au multimer@MoS_2 samples exhibit the best hydrogen gas yields, compared with those of Au monomer@MoS_2 and pure MoS_2, mainly because of the enhancement of light absorption and the improvement of exciton generation and dissociation (Figs. 5(c) and 5(d)) [113].

Even though the LSPR of 0D noble metal nanostructures can strongly boost the generation of hot electrons toward photocatalytic reactions [114], the high cost of noble metals restricts large-scale practical applications. Recently, theoretical studies have predicted that heavily-doped semiconductors (e.g., WO_{3-x}, $Cu_{2-x}S$, and MoO_{3-x}) can exhibit indirect plasmonic absorption, which is ascribed mainly to collective charge oscillation on the metal-chalcogenide surface propagated by numerous anion vacancies within the crystal lattice [115, 116]. Such an effect has been observed in hybrid photocatalysts of MoS_2/MoO_2 and MoS_2@TiO_2. For example, a Schottky junction of MoS_2/MoO_2 has been formed via calcination. The LSPR effect from MoO_2 is induced by oxygen vacancies and proper Fermi level positions. Consequently, the LSPR effect results in a broad spectral response and a significant improvement in exciton generation and dissociation. The Schottky heterostructure exhibits a 242% increment in H_2 production compared to that for MoS_2 nanosheets [117]. A nonmetal plasmonic MoS_2@TiO_2 heterostructure has been synthesized via carefully controlled anodization, physical vapor deposition, and chemical vapor deposition processes. The heterostructure exhibits the morphology of laminated MoS_2 in conjunction with TiO_2 nanocavity arrays. It can adsorb a wide spectral range, from ultraviolet–visible (UV–vis) to near-infrared (NIR) wavelengths. Moreover, it exhibits superb photocatalytic activity with an H_2 yield rate of 181 mmol/(g·h) because of the facilitated electron transfer pathway and appropriately tuned energetic position of the conduction band [118].

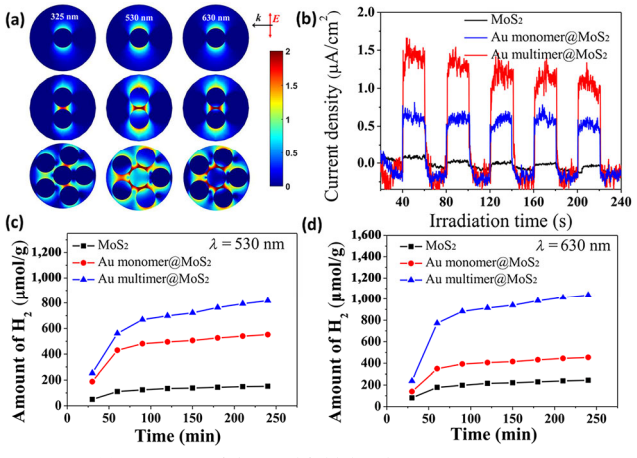

Figure 5 (a) Top views of electrical field distribution in Au monomer@MoS_2, Au dimer@MoS_2, and Au multimer@MoS_2 under different excited wavelengths. (b) Photocurrent density-time curves (λ = 325 nm) and (c) and (d) photocatalytic H_2 evolution rates (λ = 530 and 630 nm) of MoS_2 spheres, Au mononer@MoS_2, and Au multimer@MoS_2. Reproduced with permission from Ref. [113], © Elsevier B.V. 2016.

LSPR can overcome the limitations of traditional semiconductor materials that comply with energy alignment. However, there is a high potential barrier that limits hot-electron transfer at the heterostructure interface. The interface effect depends on the synthesis method. For example, the photocatalytic activity of MoS_2 or WS_2 deposited chemically on CdS is much higher than that of a mechanical mixture of MoS_2 or WS_2 and CdS [119, 120]. 2D layered TMDCs exhibit strong molecular intra-layer bonds but weak interlayer bonds [121]. This structure leads to highly anisotropic properties, for example, crystallographic orientation-dependent charge separation. That is, different crystal planes exhibit varying photon-to-current conversion efficiencies [122]. Generally, the energy alignment, crystallographic orientation, and interface contact/binding are the main factors that determine the photoactivity of 0D-2D heterostructures [123].

Transition-metal oxides, transition-metal sulfides, and their composites, such as NiS_x, WS_2, CoO, and CoP, have been used to partly or completely replace noble-metal nanomaterials. They are highly active, durable, and earth-abundant co-catalysts [124–128]. Incorporated P in transition metals can act as base sites, trapping positively charged protons, lowering the binding energy of hydrogen, and restricting electron delocalization in the metal [127]. Transition-metal sulfides as co-catalysts are beneficial for H_2 release because the surface-adsorption free energy of hydrogen on transition-metal sulfides can be near zero [125, 128]. For example, MoS_2 is a promising alternative to platinum for promoting photocatalytic hydrogen reactions on hexagonal $ZnIn_2S_4$ [129]. An atomic-level 2D heterostructure of MoS_2 quantum dots (QDs) at the S vacancies (V_S) on the Zn facet in monolayered $ZnIn_2S_4$ (V_S–M–$ZnIn_2S_4$) has been obtained via chemical exfoliation (lithium intercalation and ultra-sonication) and hydrothermal reaction (Fig. 6(a)). The lithium intercalation process leads to the construction of S vacancies in V_S–M–$ZnIn_2S_4$ nanosheets. The S vacancies as electron traps, which prevent vertical transmission of electrons, enrich electrons on the Zn facet and result in a highly efficient interface with low contact resistance. The presence of MoS_2 QDs on the S vacancy of V_S–M–$ZnIn_2S_4$ can be beneficial for the transportation of charge carriers. The heterostructure exhibits a higher photocurrent than that of V_S–M–$ZnIn_2S_4$ or bulk $ZnIn_2S_4$ (Fig. 6(b)) because the atomic level Zn–S heterointerface allows photo-generated electron transfer from V_S–M–$ZnIn_2S_4$ to MoS_2 QDs (Fig. 6(c)). In addition, this heterostructure exhibits more efficient atomic utilization, controllable charge flow, and an excellent photocatalytic hydrogen evolution activity of 6.884 mmol/(g·h), which is much higher than that of bulk $ZnIn_2S_4$ (Fig. 6(d)).

Because of their ultrathin planes, 2D TMDCs can act as effective supports for the anchoring of other semiconductor nanoparticles to avoid coalescence and agglomeration of the semiconductors. This is beneficial for maintaining the activity and stability of the photocatalysts. For example, the combination of CdS nanomaterials and TMDC nanosheets can form p/n junctions, which exhibit enhanced performance towards photocatalytic hydrogen production under visible-light irradiation. In this system, a decrease in thickness of TMDCs will further improve photocatalytic hydrogen evolution because more active sites become exposed [119]. For example, monolayers of MS_2 (M = W or Mo) have been selectively grown on the Cd-rich (0001) surface of wurtzite CdS nanocrystals via a facile one-pot wet-chemical method. The WS_2-CdS and MoS_2-CdS nanohybrids exhibit better performance in terms of hydrogen evolution rate (1.98 and 1.47 mmol/(g·h), respectively) than that of pure CdS (0.12 mmol/(g·h)) [119]. In addition,

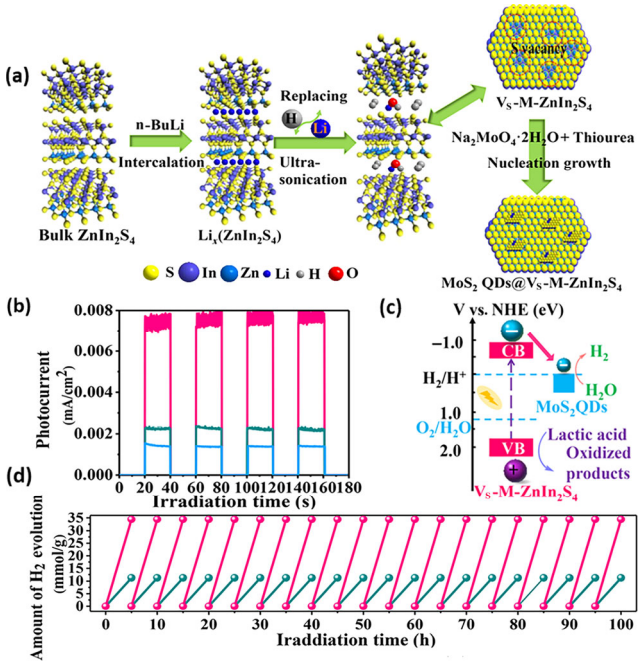

Figure 6 (a) Schematic presentation of fabrication of MoS_2 QDs@V_S–M–$ZnIn_2S_4$. (b) Transient photocurrent responses of bulk $ZnIn_2S_4$ (blue curve), V_S–M–$ZnIn_2S_4$ (green curve), and 2MoS_2 QDs@V_S–M–$ZnIn_2S_4$ (red curve). (c) Band alignment of 2MoS_2 QDs@V_S–M–$ZnIn_2S_4$. (d) Recycling H_2 evolution tests of V_S–M–$ZnIn_2S_4$ (green line) and 2MoS_2 QDs@V_S–M–$ZnIn_2S_4$ (red line). Here, MoS_2QDs@V_S-M-$ZnIn_2S_4$ nanocomposites with different amounts of MoS_2QDs were labeled as *x*MoS_2QDs@V_S–M–$ZnIn_2S_4$; V_S–M–$ZnIn_2S_4$ represents the S vacancies on a Zn facet in monolayered $ZnIn_2S_4$. Reproduced with permission from Ref. [129], © American Chemical Society 2018.

after simple functionalization (e.g., element doping and structure defects), either main catalysts or co-catalysts can further improve photocatalytic properties [130, 131]. The main reason is that surface functionalization allows precise control of the surface electronic states. For example, metal atom-doped MoS_2 nanosheets synthesized via hydrothermal reactions exhibit better stability, hydrogen production efficiency, and photocatalytic activity, with a hydrogen production rate of 2.695 mmol/(g·h) [131]. The presence of S vacancies and O atoms in MoS_2 nanosheets can reduce the energy barrier for H_2 evolution and improve electric conductivity. Therefore, the photoactivity of CdS nanocrystals can be further improved via combination with defect-rich 2D MoS_2 as an effective co-catalyst for photocatalytic H_2 production [132]. After defect-rich O-incorporated 1T-MoS_2 nanosheets are combined with CdS nanorods via hydrothermal reactions, the resulting material exhibits an extraordinary photocatalytic H_2 production rate of 132.4 mmol/(g·h) under visible light (λ > 420 nm) [133]. The heterostructure of irregular CdS nanospheres hybridized with oxygen-incorporated defect-rich MoS_2 ultrathin nanosheets exhibits a quantum yield of ~ 22% at 420 nm and an H_2 generation rate of ~ 17.2 mmol/(g·h) under visible light, which is much higher than that of CdS (~ 0.36 mmol/(g·h)) or 3 wt.% Pt/CdS (~ 1.17 mmol/(g·h)). The defects in the MoS_2 nanosheets, including S atoms on the exposed plane edge, provide additional active sites, whereas the incorporation of O atoms leads to a decrease in the band gap. Therefore, such structural defects reduce the energy barrier for H_2 evolution and improve the electrical conductivity of MoS_2. In addition, intimate interfaces between the CdS irregular nanospheres and defect-rich MoS_2 ultrathin nanosheets allow high-efficiency charge transfer and prevent the recombination of electron–hole pairs [134].

Other non-noble-metal or metal-free nanomaterials, including elemental semiconductors (e.g., silicon, red phosphorus, black phosphorus), conjugated polymers, hexagonal boron nitride, g-C_3N_4, carbon nanotubes, graphene quantum dots, graphene oxide (GO) quantum dots, and their element-doped types, have been widely used in photocatalytic water splitting [135–137]. Most conductive carbon nanomaterials (e.g., carbon nanotubes and graphene) are zero-bandgap and non-photoactive materials. However, their band gaps can be opened via size modulation and chemical modification, thus destroying their symmetry. For example, nitrogen-doped graphene-oxide quantum dots deposited with Pt exhibit high activity for H_2 generation with 12.8% of quantum yield under visible light irradiation (λ = 420 nm). GO with a tunable band gap dependent on the amount of O atoms can facilitate an oxygen evolution reaction. However, GO suffers from photochemical reduction, and thus its photoactivity decays [138]. For GO semiconductor, nitrogen doping extends the resonant π-conjugation to prolong the charge lifetime. Sulfur doping can break the electron neutrality to facilitate charge transfer [139]. Generally, metal-free nanomaterials are used to combine with other 2D semiconductors to improve their photoactivity [140–142]. For example, the combination of g-C_3N_4 and transition-metal sulfides can significantly decrease the Gibbs free energy of H_2 adsorption, improve the separation efficiency of photo-generated carriers, and produce more reaction-active sites [143]. Carbon quantum dots (CQDs) can reduce the band gaps of semiconductor materials so that more reactive oxygen species can be generated by light [144]. A strong interaction between semiconductors and CQDs can stabilize the interface and facilitate the charge transfer process. Hence photocatalytic performance is enhanced [145].

Compared with binary TMDCs, ternary chalcogenides (e.g., $CuGaS_2$ and $Cd_xZn_{1-x}S$) and quaternary chalcogenides (e.g., Cu_2ZnSnS_4) exhibit higher photocatalytic activity and stability against photo-corrosion [146, 147]. For example, ZrSeS and HfSeS monolayers exhibit higher carrier mobility than that of ZrSe and HfSe [148]. A sandwiched S-Mo-Se structure (Janus SMoSe) fabricated via the reaction of one Se layer of monolayer $MoSe_2$ with vaporized sulfur demonstrates better performance than that of pure MoS_2 or $MoSe_2$ in terms of the hydrogen evolution reaction (HER) because of the presence of strain and defects [148, 149]. In addition to their composition, changes in spatial structure of 0D nanomaterials can result in completely different properties and functions [86]. For example, core/shell nanoparticles exhibit controllable properties which can be regulated via changes in either the constituting materials or the core-to-shell ratio [150]. Because of the coating of the shell material, the properties of the core particle can be modified to improve the overall stability, photocatalytic reactivity, and dispersibility of the hybrid photocatalysts.

Recently, the size of 0D photocatalysts, especially in extreme situations, has been attracting research interest in the field of photocatalysis [151]. For example, single-atom photocatalysts can realize the maximum utilization of atoms in a catalytic reaction because of the coordinatively unsaturated state of the active center and its stable coordination with the support [152]. In hybrid photocatalysts, the size of 0D nanomaterials varies from quantum dots over clusters and molecules down to single atoms. Both theoretical and experimental results have demonstrated that a decrease in size is beneficial for improving photoactivity and/or selectivity because it enhances light-harvesting, charge transfer dynamics, and surface reactions of a photocatalytic system. For 2D layered materials as supports or substrates, single atoms may be embedded into the defects of supports, act as dopants to replace surface atoms, or bond with surface atoms of 2D layered materials [153]. In this review article, single-atom photocatalysts mainly refer to

the last case, namely single atoms anchored on the surface of 2D TMDCs. A decrease in size from a nanocrystal to a single atom can effectively regulate atomic and electronic structures and active sites [154]. A suitably small particle size allows more active sites to be exposed and benefits the transfer of photo-generated charges from other photo-excited semiconductors to surface reaction sites. Thus, the recombination probability is decreased [155]. Systems of single atom/2D materials are mainly nanocomposites of metal atoms and g-C_3N_4, graphene, graphene oxide, or metal-organic framework materials [156, 157]. In particular, singly dispersed metal atoms anchored on N/C-based materials (e.g., graphene, graphene oxide, and g-C_3N_4), referred to as M-N-C nanomaterials, have been the most extensively investigated [158–161]. However, 2D TMDCs are rarely used to construct single-atom hybrid photocatalysts; therefore, more attention should be paid to this in future research.

4.2 1D–2D hybrid heterostructures for water splitting

1D material systems are regarded as the smallest-dimension structures for efficient transport of electrons and optical excitation [166]. The possible structures of 1D–2D hybrid heterostructures are shown in Fig. 7(a). Small-size 2D nanosheets can grow vertically or wrap the surface of relatively large-size 1D nanomaterials, whereas small-size 1D materials adhere to the surface of 2D materials. The morphology of vertically aligned 2D nanosheets on 1D nanomaterials leads to the exposure of almost the entire surface and maximizes active sites at the edges for photocatalytic reactions [167].

In terms of charge separation and transfer, 1D–2D hybrid heterostructures possess more advantages than 0D–2D hybrid heterostructures because of their large contact area. Similar to 0D nanomaterials, 1D nanomaterials can effectively prevent the aggregation of 2D nanomaterials and act as co-catalysts to enhance the photoactivity of 2D nanomaterials. For example, porous TiO_2 nanowires have been coated by MoS_2 nanosheets via a hydrothermal method, forming a 0D–2D hybrid heterostructure with a shell–core nanostructure (Fig. 7(b)). TiO_2 nanowires, as a robust substrate, allow MoS_2 nanosheets to present more active sites at their plane edges. After the incorporation of Eosin Y, the heterostructure of MoS_2 nanosheet/porous TiO_2 nanofiber exhibits high activity under visible light because of dye sensitization. As shown in Fig. 7(c), this heterostructure catalyzes the hydrogen evolution reaction at a rate of 16.7 mmol/(g·h) [168]. Via a simple hydrothermal reaction, MoS_2 nanosheets can be made to vertically stand on CdS nanowires. This structure provides MoS_2 nanosheets with a high exposure of active edge sites and increases the charge separation and transfer rate. The best photocatalytic H_2 evolution rate (9.73 mmol/(g·h)) is obtained when MoS_2 is loaded at 10 wt.%, and a quantum yield of 60.3% at 420 nm can be reached [167].

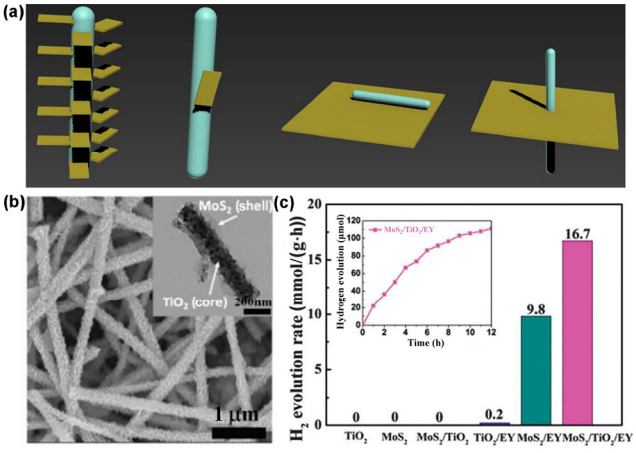

Figure 7 (a) Schematic illustration of 1D-2D hybrid heterostructures. (b) Morphology characterization of MoS_2 nanosheet/TiO_2 nanowire heterostructures and (c) photocatalytic hydrogen evolution rates of different photocatalytic systems. Reproduced with permission from Ref. [168], © The Royal Society of Chemistry 2014.

Other 1D–2D hybrid heterostructures (Table 2), such as MoS_2 nanosheet/TiO_2 nanofiber [169], 2D hierarchical MoS_2 nanospheres on 1D CdS nanorods [170], and CdS nanowire/$CdIn_2S_4$ nanosheets [171], all exhibit enhanced photocatalytic activity for water splitting compared with their single components or units. For example, MoS_2 nanosheets grown on the surface of TiO_2 nanowires with intimate contact can enhance electron transfer and improve structural stability [169]. The main reason is that such 1D/2D structure maximally exposes

Table 2 Typical 1D–2D hybrid heterostructures as visible-light-driven photocatalysts for water splitting[a]

Sample	Main synthesis methods	Roles of 2D TMDC	Light source	H_2 (mmol/(g·h))	Ref.
TiO_2 NW/MoS_2 NS	Hydrothermal method	Co-catalyst, active sites	300 W Xe lamp (λ > 420 nm)	16.7	[168]
TiO_2 NF/MoS_2 NS	Hydrothermal method	Active sites	300 W Xe lamp (λ > 420 nm)	0.49	[169]
$Zn_{1-x}Cd_xS$/D-ZnS(en)$_{0.5}$	Solvethermal synthesis	Inducing defect states excitation, broadening the light absorption spectrum	300 W Xe lamp (λ > 420 nm)	15.45	[172]
CdS/MoS_2	Hydrothermal reaction	Co-catalyst, active edge sites	300 W Xe lamp (λ > 420 nm)	9.73	[167]
CdS/MoS_2	Hydrothermal synthesis	Enhancement of visible light absorption	100 W Xe lamp (λ > 420 nm)	11.85	[170]
MoS_2/TiO_2	Hydrothermal treatment	Electron mediator and transporter	350 W Xe lamp (λ > 420 nm)	0.075	[173]
MoS_2/TiO_2	Hydrothermal method	Cocatalyst, trapping electrons	300 W Xe lamp (λ > 420 nm)	10.04	[174]
CdS NW/$CdIn_2S_4$ NS	Solvent mediated, surface reaction-driven growth route	Main catalyst	300 W Xe lamp ($\lambda \geq$ 420 nm)	0.823	[171]
CdS/$CoMoS_4$	Cation exchange method	Active sites	300 W Xe lamp (λ > 420 nm)	0.2	[175]
WS_2/CdS	Chemical exfoliation	Active sites, sacrificial electron donor	300 W Xe lamp (λ > 420 nm)	11.41	[176]

[a]NP, nanoparticle; NS, nanosheet; QD, quantum dot; NW, nanowire; NF, nanofiber. D and en in D-ZnS(en)$_{0.5}$ represent defect-rich and ethylenediamine, respectively.

the active edge sites of 2D materials. As a result, the synergetic effect between MoS_2 nanosheets and TiO_2 nanofibers leads to a high photocatalytic hydrogen production rate of 0.49 mmol/(g·h). On the other hand, a 1D/2D heterostructure of $Zn_{1-x}Cd_xS$/D-$ZnS(en)_{0.5}$ (en = ethylenediamine) has been fabricated via a one-pot synthesis method (Fig. 8(a)). Because of effective interfacial and interior carrier separation, this heterostructure possesses superior photoactivity after further optimizing the molar ratio of Cd/(Cd + Zn) to 0.24. 1D $Zn_{0.41}Cd_{0.59}S$ nanorods uniformly adhere to 2D D-$ZnS(en)_{0.5}$ nanosheets. The heterostructure exhibits certain stability (Fig. 8(b)), and the photoactivity is slightly degraded even after six consecutive runs [172]. The hybrid heterostructure has an H_2 evolution rate of 15.45 mmol/(g·h) under visible light irradiation (Fig. 8(c)). Meanwhile, a type II heterostructure of CdS nanowire/$CdIn_2S_4$ nanosheet has been synthesized by a new solvent-mediated, surface reaction-driven growth route. The heterostructure has better photocatalytic activity (0.823 μmol/(g·h)) for H_2 production than that of $CdIn_2S_4$ nanosheets (145 μmol/(g·h)) or CdS nanowires (84 μmol/(g·h)), mainly because of its large specific surface area, efficient optical absorption, and facile separation of charge carriers [171].

4.3 2D–2D hybrid heterostructures for water splitting

Using vdW forces to construct 2D–2D heterogeneous photocatalysts offers an alternative low-energy material-integration approach. In general, 2D–2D heterogeneous photocatalysts include vertical (out-of-plane) and lateral (in-plane) 2D junctions [177]. The former is more frequently used in constructing highly effective photocatalysts. The reason is that the interfaces of semiconductor-based hybrid photocatalysts significantly affect photoactivity [178]. The small contact area at the interface of co-catalyst/semiconductor cannot effectively generate an electric field. Compared with 0D–2D and 1D–2D hybrid heterostructures, vertical 2D–2D hybrid heterostructures possess larger interface area, which is beneficial for the efficient capture of light energy and interfacial charge separation [179, 180].

Artificially stacking 2D–2D heterostructure is a flexible route for designing photocatalysts, involving only changes in composition and layer sequence without stringent lattice-matching requirements (Table 3) [181]. For example, with graphene used as a substrate, MoS_2 and WSe_2 monolayers can be well aligned in a symmetry- equivalent orientation, even though MoS_2/graphene and WSe_2/graphene exhibit a lattice mismatch of > 20% [182]. Strong covalent bonds provide in-plane stability to 2D crystals, whereas relatively weak vdW forces are sufficient to keep the stacking nanosheets together [183]. Furthermore, charge redistribution and induced structural changes may occur between neighboring (and even more distant) crystals in the stack, which can strongly affect the surface or interface reactions. Because of non-passivated edge states (imbalance charges), the energy band structure of 2D–2D heterostructures would change at the edges. This is similar to surface/interface band bending in conventional 3D materials [184]. For example, in MoS_2-WS_2 vdW heterostructures, N-doping raises the edge band, whereas P-doping leads to a decline of the edge band [184].

For 2D–2D vdW heterostructures with large intimate interfaces, the main synthesis methods include ultrasonic absorption [185], hydrothermal method [186, 187], electrostatic self-assembly [188], and chemical vapor deposition [189]. Because of the special structure of 2D–2D vdW heterostructures, their interfaces between neighboring 2D layers or between 2D overlayers and substrate surfaces can effectively regulate the microenvironment around the active sites and activate the inert plane (without any dangling bonds) via confined effects [96, 97]. The confined effects can be observed in 2D nanospaces, where some reactions are faster than in open systems. It is

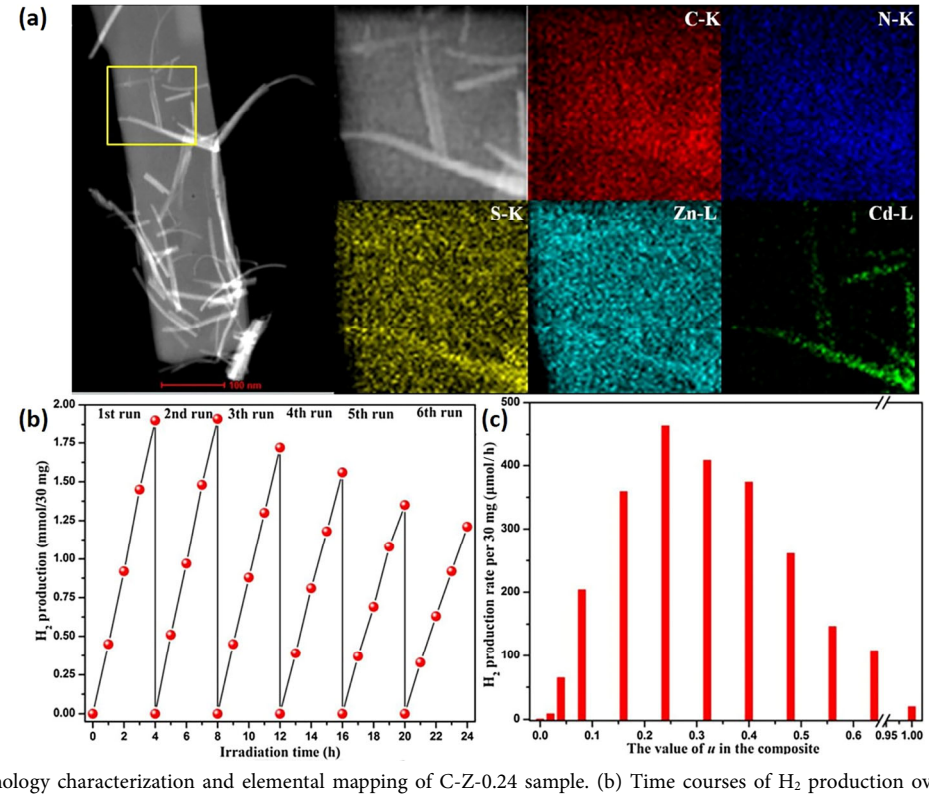

Figure 8 (a) Morphology characterization and elemental mapping of C-Z-0.24 sample. (b) Time courses of H_2 production over C-Z-0.24 composite under visible light irradiation (λ > 420 nm). (c) Photocatalytic H_2 evolution rates of all C-Z-u under visible light irradiation (λ > 420 nm). Pure CdS and D-$ZnS(en)_{0.5}$ are labeled as C and Z, respectively. A series of $Zn_{1-x}Cd_xS$/D-$ZnS(en)_{0.5}$ heterostructures are abbreviated as C-Z-u (u is the molar ratio of Cd/(Cd + Zn) in each composite). Reproduced with permission from Ref. [172], © Elsevier B.V. 2018.

Table 3 Typical 2D–2D heterostructures as visible-light-driven photocatalysts for water splitting[a]

Sample	Type	Main synthesis methods	Light source	H_2 (mmol/(g·h))	Ref.
2H-MoS_2/1T'- MoS_2	Type I	Exfoliation, thermal annealing	200 W Hg lamp (λ > 400 nm)	1.5	[192]
WO_3/$ZnIn_2S_4$	Z-scheme	Hydrothermal, calcination	300 W Xe lamp (λ > 420 nm)	2.2	[204]
MoS_2-graphene/$ZnIn_2S$	Z-scheme	Hydrothermal	300 W Xe lamp (λ > 420 nm)	4.17	[196]
CdS/MoS_2	p–n	Ultrasonic adsorption	300 W Xe lamp (λ > 400 nm)	1.75	[185]
CdS/MoS_2	p–n	Sonication	300 W Xe lamp (λ > 420 nm)	140	[205]
$ZnIn_2S_4$/$MoSe_2$	—	Electrostatic self-assembly	300 W Xe lamp (λ > 400 nm)	6.45	[203]
MoS_2/$ZnIn_2S_4$	—	*In situ* self-assembly	300 W Xe lamp (λ > 400 nm)	8.90	[104]
MoS_2-graphene/$ZnIn_2S_4$	—	Hydrothermal reaction	300 W Xe lamp (λ > 420 nm)	4.17	[196]
g-C_3N_4/MoS_2	—	Impregnation/sulfidation	300 W Xe lamp (λ > 420 nm)	0.02	[206]
g-C_3N_4/$ZnIn_2S_4$	Type I	Hydrothermal	300 W Xe lamp (λ > 420 nm)	2.78	[207]
MoS_2/$Bi_{12}O_{17}Cl_2$	—	Vigorous stirring/reflux	300 W Xe lamp (λ > 420 nm)	33	[208]
$ZnIn_2S_4$/MoS_2	—	Solvothermal process	300 W Xe lamp (λ > 420 nm)	0.08	[209]
V_S-$ZnIn_2S_4$/WO_3	Z-scheme	Lithiation reaction	300 W Xe lamp (λ > 420 nm)	11.09	[210]

[a]1T'-MoS_2, quasi-metallic MoS_2; V_S-$ZnIn_2S_4$, sulfur-vacancy-confined-in $ZnIn_2S_4$; —, the data are not available.

well known that in addition to the active sites, the microenvironments around the active sites are equally important for catalytic performance in heterogeneous catalysis. 2D TMDCs over other 2D materials, or *vice versa*, can strongly affect the physicochemical properties. For example, the surface of 2D MoS_2 is covered by a high-K dielectric material, which can significantly improve the mobility via suppression of Coulomb scattering [190]. In addition, a 2D cover can help stabilize active sites and modulate chemistry at these sites [191] because the 2D nano-spacing weakens adsorption energy for surface reactions. Because of confinement effects, the surface chemistry and catalysis are strongly modulated by 2D covers. Typical 2D–2D vdW heterostructures include conductor–semiconductor (e.g., reduced graphene oxide-CdS), semiconductor–semiconductor (e.g., CdS/MoS_2), and their mixtures (e.g., MoS_2-graphene/$ZnIn_2S$) [185, 188, 192, 193].

The most typical examples of conductor–semiconductor 2D–2D vdW heterostructures are semiconductor/graphene vdW heterostructures. The potential of graphene (−0.08 V, pH = 0) is normally lower than the conduction-band potential of semiconductor photocatalyst. Thus, electrons transfer from the semiconductor to the graphene surface, which improves the electron–hole separation. Graphene can enhance light absorption to produce heat and create a unique photothermal effect around the photocatalyst surface. However, the loading amount of graphene needs to be carefully optimized because overloading graphene leads to light-shielding effects, significantly suppressing the light absorption of the photocatalysts [36]. The large specific surface area of graphene is also beneficial for providing a greater number of active sites. Graphene as a 2D cover can regulate the microenvironments of 2D semiconductors in spite of weak vdW forces between them. For example, the conduction-band potential of a semiconductor can be shifted by combination with graphene [71, 181, 194].

Interface effects play a critical role in heterocatalysis. In particular, the built-in electric fields or the space charge layer in these stacks can split the excitons and suppress charge recombination [100]. For example, 2D MoS_2 has negligible photocatalytic activity due to insufficient charge separation, even though bulk MoS_2 has an indirect absorbance edge at ~ 1,040 nm [186, 195]. When p-type MoS_2 nanoplatelets are deposited on n-type N-doped reduced graphene oxide (n-N-rGO) to form a p-MoS_2/n-N-rGO heterostructure, the photocatalytic activity toward H_2 production is significantly improved. This is achieved in the wavelength range from UV through NIR light. The main reason is that the p–n junction can significantly enhance charge generation and suppress charge recombination [186]. The addition of other nanocrystal semiconductors, metals, or photosensitizers on/in 2D–2D heterostructures can further improve their photoactivity [196, 197]. Such complex material systems can be well understood using the three types of heterostructures discussed previously.

Semiconductor–semiconductor vdW heterostructures are constructed using mainly 2D oxides or sulfides as building blocks [198]. This is a viable way of relieving aggregation, increasing optical absorption, and improving photocatalytic efficiency. Most semiconductors cannot produce high activity for H_2 evolution without a co-catalyst, even in the presence of a sacrificial electron donor. To some extent, the presence of co-catalysts can prevent the recombination of electron–hole pairs and accelerate surface reactions [199]. Stacking monolayer 2D materials on top of each other is similar to the intercalation of layered exotic species into the vdW gap of layered materials. Intercalation can lead to a decoupling state for layered bulk materials. For example, an interlayer spacing expansion of 7% in MoS_2 has been reported to be sufficient for decoupling adjacent MoS_2 mono-layers, causing each MoS_2 monolayer in the composites to behave similarly to a freestanding MoS_2 monolayer [200]. The intercalation of exotic species into bulk or multi-layer TMDCs can cause a transition from indirect-gap to direct-gap semiconductors and decoupling of the interlayer interaction. DFT calculations show that MoS_2/$MoSe_2$/MoS_2 tri-layer heterostructures induce a direct bandgap of 0.69 eV, where the valence band maximum (VBM) at the K point is mainly from the $MoSe_2$ layer. The conduction-band minimum (CBM) at the K point is attributed mainly to the MoS_2 layer [142]. Such a band structure is favorable for the separation of electron–hole pairs [201].

Semiconductor–semiconductor vdW heterostructures can realize efficient separation and transfer of charge carriers, accelerate the surface proton reduction with abundant active sites, and improve visible-light absorption. Combining 2D TMDCs with 2D $ZnIn_2S_4$ is advantageous for solar hydrogen generation because of the suitable band gap (~ 2.40 eV) of 2D $ZnIn_2S_4$ and considerable chemical stability [104, 196, 202, 203]. For example, semiconductor–semiconductor vdW heterostructures, such as $ZnIn_2S_4$/$MoSe_2$ and $ZnIn_2S_4$/MoS_2, exhibit better photoactivity than that of pure $ZnIn_2S_4$ or MoS_2 [104, 196, 202, 203]. A $ZnIn_2S_4$/$MoSe_2$ vdW heterostructure (Figs. 9(a) and 9(b)) obtained via a highly scalable self-surface charge

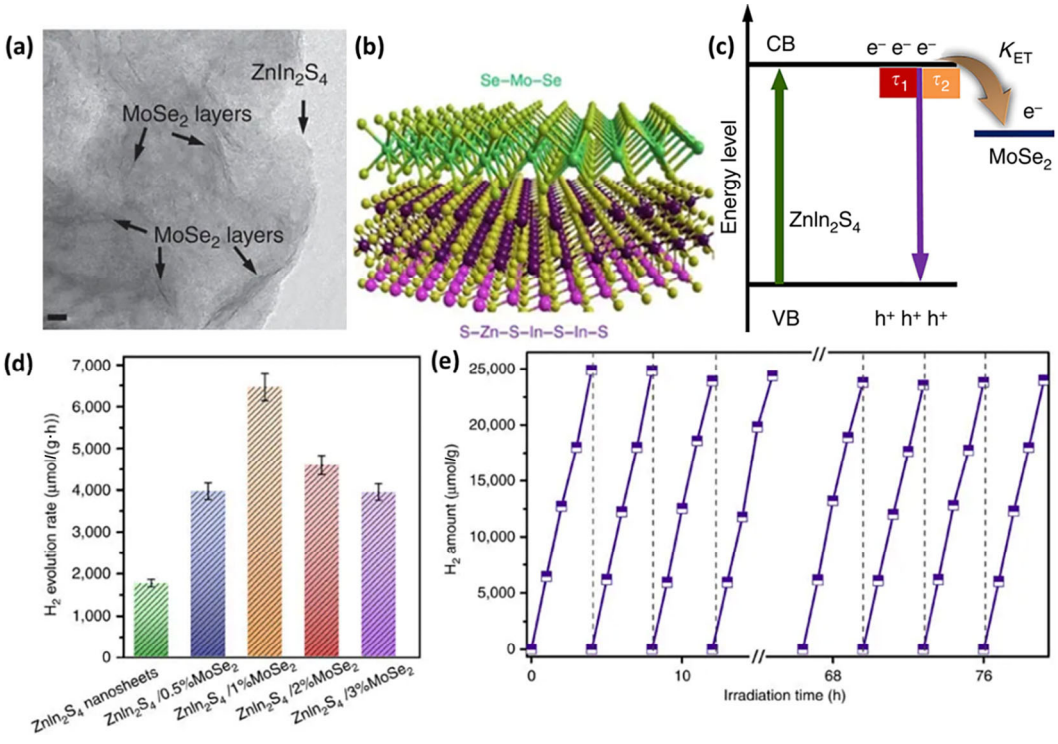

Figure 9 Transmission electron microscopy (TEM) image (a), atomic structure (b), and schematic illustration of interfacial charge carrier transfer (c) of hetero-layered $ZnIn_2S_4/MoSe_2$. (d) Photocatalytic H_2 evolution over $ZnIn_2S_4/MoSe_2$ composites with different weight ratios of $MoSe_2$. (e) Recycling photoactivity test of $ZnIn_2S_4$/1%$MoSe_2$. Reproduced with permission from Ref. [203], © Yang, M. Q. et al. 2017.

exfoliation and electrostatic coupling approach exhibits an obvious improvement in terms of photocurrent. This is due to the benefits of hetero-layered $ZnIn_2S_4/MoSe_2$ for the separation and transportation of photo-generated charge carriers (Fig. 9(c)). Under optimal conditions, a $ZnIn_2S_4/MoSe_2$ vdW heterostructure ($ZnIn_2S_4$/1%$MoSe_2$) exhibits the best H_2 evolution rate of 6.45 mmol/(g·h), which is considerably higher than that of $ZnIn_2S_4$ nanosheets or other $ZnIn_2S_4/MoSe_2$ composites (Fig. 9(d)). In addition, the $ZnIn_2S_4/MoSe_2$ vdW heterostructure has excellent stability with negligible loss in photoactivity (Fig. 9(e)) after 20 consecutive cycles and 80 h under visible-light irradiation.

4.4 Other mixed-dimensional heterostructures for water splitting

In addition to 0D–2D, 1D–2D, and 2D–2D heterostructures, another strategy is to design complex mixed-dimensional heterostructures with hierarchical architectures and multiple components. These can minimize the drawbacks and maximize the advantages of the individual components [196, 211–214]. In multi-component complex heterostructures, three or more types of highly-efficient co-catalysts are used to enhance the photocatalytic activity (Table 4). For example, nanocomposites of MoS_2-graphene as a highly-efficient co-catalyst can enhance the photocatalytic activity of 2D $ZnIn_2S_4$ under visible-light irradiation [196]. In addition, heterostructures of Pt-loaded g-C_3N_4 nanosheets and hydrogen-treated WO_3 nanosheets exhibit a better photocatalytic H_2 generation activity of 862 μmol/h. This activity is much higher than that of g-C_3N_4/WO_3 composites because of a strong affinity and synergistic coupling effect between the two types of nanosheets, with a huge percentage of coordinated unsaturated surface atoms [212]. Most of the multi-component heterostructures are used to construct Z-scheme photocatalytic systems, which have more

Table 4 Complex mixed-dimensional heterostructures as visible-light-driven photocatalysts for water[a]

Sample	Type	Main synthesis methods	Light source	Yield (mmol/(g·h))		Ref.
				H_2	O_2	
MoS_2-CdS/Co_3O_4-$BiVO_4$	Z-scheme	Mpregnation and hydrothermal method	300 W Xe lamp (λ > 400 nm)	0.015	0.007	[218]
CdS@MoS_2@Co-Pi	—	Solvothermal and photodeposition method	300 W Xe lamp (λ > 400 nm)	40.5	—	[219]
g-$C_3N_4/MoS_2/Ag_3PO_4$	Z-scheme	Self-assembly	300 W Xe lamp (λ > 420 nm)	—	0.23	[220]
$MoS_2/Ag/Ag_3PO_4$	Z-scheme	Impregnation and chemical precipitation method	300 W Xe lamp (λ > 400 nm)	—	10.28	[221]
PtS-$ZnIn_2S_4/WO_3$-MnO_2	Z-scheme	Self-assembly	300 W Xe lamp (800 nm > λ > 420 nm)	14.85	5.6	[215]
MoS_2-CdS/WO_3-MnO_2	Z-scheme	Selective deposition	300 W Xe lamp (800 nm > λ > 420 nm)	0.0005	0.0002	[222]
CdS/$MoS_2/ZnIn_2S_4$	Z-scheme	Solvothermal reaction	300 W Xe lamp (λ > 420 nm)	2.1	—	[214]
g-C_3N_4/Ag/MoS_2	Z-scheme	Photodeposition method	300 W Xe lamp (λ > 420 nm)	0.1	—	[213]
MoS_2/graphene-CdS	—	Solution-chemistry method	300 W Xe lamp (λ > 420 nm)	6.1	—	[223]

[a]Pi, phosphate; —, the data are not available.

advantages in improving photoactivity than Schottky junctions or type I and type II heterostructures. For example, multi-component Z-scheme photocatalytic systems can achieve overall water splitting faster at a low cost in electron energy loss via a combination of two narrow-bandgap semiconductors [213, 214]. In addition, they can demonstrate a wide absorption range, long-term stability, high charge-separation efficiency, and strong redox ability, representing an improvement over single-component photocatalysts [59].

The recent development of the Z-scheme system has suggested that electron transfer between the two photocatalysts is the rate-determining process. Therefore, the presence of an electron transporter is critical to boosting electron relay. Based on the type of electron transfer between them, Z-scheme photocatalysts can be divided into shuttle redox mediators (e.g., Fe^{3+}/Fe^{2+}, IO_3^-/I^-, NO^{3-}/NO^{2-}), solid-state electron mediators (e.g., graphene), and direct systems. For example, a $[Co(bpy)_3]^{3+}/[Co(bpy)_3]^{2+}$ redox couple is used as an electron mediator for water splitting via the combination of MoS_2/CdS for water reduction and Co_3O_4/$BiVO_4$ for water oxidation. Under visible-light irradiation, the H_2 and O_2 evolution rates are 145 and 71 μmol/(g·h), respectively. However, the hybrid photocatalysts suffer from poor stability because of photocorrosion of CdS [215].

Compared with ionic redox couples, solid electron mediators are more favorable for improving photoactivity via fast transfer of electrons from an O_2 evolution photo-catalyst to a H_2 evolution photocatalyst [44, 59, 179, 216]. In addition, solid electron mediators can better avoid undesirable reverse reactions involving redox mediators and decrease light loss because the redox mediators can strongly absorb visible light [217]. For Z-scheme photocatalysts with solid-state electron mediators (or conductors) and direct systems, their structures are concluded to be photosystem I–conductor–photosystem II (PS-C-PS) and photosystem I–photosystem II (PS-PS). All-solid-state Z-scheme photocatalytic systems can reduce the distance of electron transfer, prevent side reactions between redox mediators and carriers, and remove the shielding effect of irradiated incident light caused by the redox pair [59]. The energy required to drive each photocatalyst is reduced in the Z-scheme photocatalytic systems; as a result, visible light can be utilized more efficiently in such systems than in conventional one-step water-splitting systems [216]. For the PS-C-PS system, the solid-electron mediators may be metal (e.g., Au, Ag, and Cu), nonmetal (e.g., graphene), or metal oxide (e.g., indium tin oxide) nanomaterials. For the PS-PS system, the properties of the solid–solid contact interface between PS II and PS I determine the resistance level of electron transfer. In general, both PS-PS and PS-C-PS are strongly dependent on the method of formation of the contact interface. For example, a solid–solid contact interface formed via chemical methods is more stable than that obtained via physical methods [59, 215]. Both PS-PS and PS-C-PS can better realize water splitting even without sacrifice reactants [218]. For example, PtS-$ZnIn_2S_4$/WO_3-MnO_2 nanocomposites have been synthesized via self-assembly of hexagonal $ZnIn_2S_4$ nanosheets in the presence of WO_3 and selective deposition with PtS. The hybrid photocatalyst is involved in a direct Z-scheme photocatalytic system (Fig. 10(a)) and exhibits photocatalytic activity for water splitting under visible light. The efficiency of the Z-scheme charge transfer pathway strongly depends on the interface between $ZnIn_2S_4$ and WO_3. Optimum activity has been obtained over 0.5%PtS-20%$ZnIn_2S_4$/WO_3-3.0%MnO_2 with an H_2-evolution rate of 14.85 μmol/(g·h) and an O_2-evolution rate of 6.6 μmol/(g·h) in pure water without any sacrificial agent (Fig. 10(b)). On the

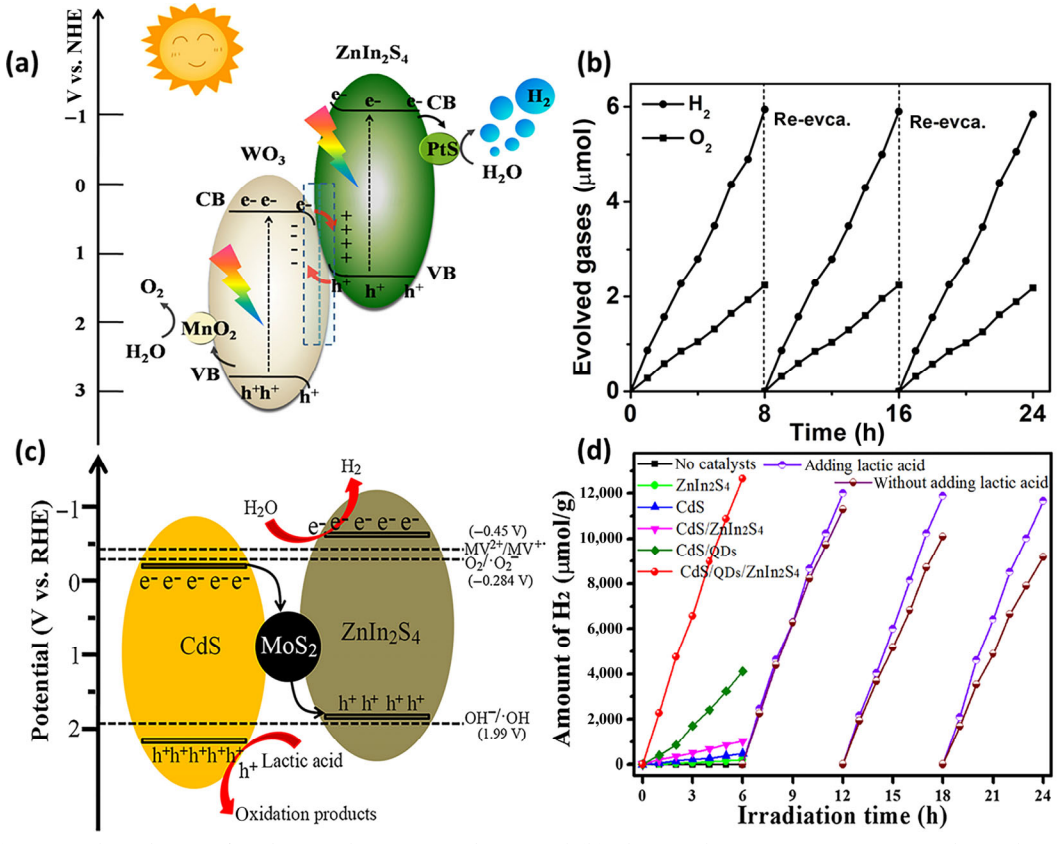

Figure 10 (a) Proposed mechanism for photocatalytic water splitting and (b) photocatalytic activity over water splitting based on 0.5%PtS-20%$ZnIn_2S_4$/WO_3-3.0%MnO_2 nanocomposite (reproduced from Ref. [215] with permission, © Elsevier B.V. 2019). (c) Photocatalytic mechanism for photocatalytic water splitting based on CdS/MoS_2 QDs/$ZnIn_2S_4$ hybrid nanocomposites and (d) photocatalytic activity for hydrogen evolution of as-prepared samples from water splitting with or without lactic acid as sacrificial agent (reproduced from Ref. [214] with permission, © Elsevier B.V. 2020).

other hand, Z-scheme CdS/MoS_2 QDs/$ZnIn_2S_4$ architectures have been synthesized via solvothermal or hydrothermal methods. Here, MoS_2 QDs function as a solid-state electron medium; the photo-generated electrons transfer from the CB of CdS to MoS_2 QDs and then migrate to the VB of $ZnIn_2S_4$. They then recombine with the photo-generated holes on the VB of $ZnIn_2S_4$. Meanwhile, the rest of the photo-generated charges possess a strong redox ability for water splitting (Fig. 10(c)). The multi-component Z-scheme photocatalysts exhibit synergetic effects in improving hydrogen evolution under visible light even without lactic acid as a sacrificial agent because MoS_2 QDs not only inhibit carrier recombination but also regulate the flow direction of photo-generated charges. The Z-scheme CdS/MoS_2 QDs/$ZnIn_2S_4$ hybrid photocatalyst exhibits a higher H_2-evolution rate (2,107.5 μmol/(g·h)) than those of bare CdS nanorods and pure $ZnIn_2S_4$ nanosheets (Fig. 10(d)). Because the energy required to drive each photocatalyst is reduced in Z-scheme photocatalytic systems, visible light can be utilized more efficiently in such systems than in the conventional one-step water-splitting systems.

5 Conclusion and outlook

In this review, we mainly discussed the advantages of 2D TMDCs and their applications for photocatalytic water splitting under visible-light irradiation. We highlighted strategies and typical examples of improving the photoactivity of 2D TMDCs. Although extensive research progress has been made in the field of 2D nanomaterials, challenges in 2D TMDC-based photocatalysis remain. Controlled synthesis and design of 2D TMDC-based heterostructures, especially regarding material dimensionality (e.g., thickness), composition, and surface features (e.g., atom arrangement and defects), still require substantial research efforts in the future. Compared with the graphene family, especially graphene, g-C_3N_4, and graphene oxide, 2D TMDCs are still in their infancy in the realm of visible-light-driven photocatalysts for water splitting. As summarized, most visible-light-driven photocatalysts still focus on photocatalytic hydrogen production; by contrast, photocatalysts for oxygen evolution or overall water splitting are still rarely reported. Therefore, for 2D TMDC-based photocatalysts, the challenge remains of developing dual co-catalysts and to realize overall water splitting under visible-light irradiation. In addition, other difficulties include simultaneous regulation of stability and high photoactivity (or high quantum efficiency), better combination of water remediation (e.g., pollutants' mineralization) and water splitting, and reduction of the environmental risks of nanocrystal photocatalysts. To a large extent, such problems can be solved via the synthesis of photocatalytic materials by low-cost, controllable, mass-production methods.

In the long term development, 2D–2D vdW heterostructures and/or single-atom hybrid photocatalysts will gain more attention for their capability to achieve high-performance water splitting. Z-scheme 2D–2D vdW heterostructures provide a flexible way of controlling physicochemical properties via stacking of 2D materials together in different rotational, translational, and stacking geometries. In addition, single-atom photocatalysts can fully take advantage of catalysts and lower the recombination of photogenerated electron–hole pairs, but their stability and controllable synthesis need to be improved. The surface chemistry of 2D TMDCs is crucial in processes such as photochemical water-splitting because it can make the entire basal plane, rather than just the edges of 2D TMDCs, catalytically active. Therefore, further efforts may be focused on *in-situ* characterization techniques to gain a deeper understanding of the surface or interface processes. Lastly, *ab initio* simulations based on DFT can provide information on some critical factors as bandgap, band edge levels, optical absorption, and charge carrier mobility, which also help experimentalists to screen promising photocatalytic nanomaterials.

Acknowledgements

The authors acknowledge the financial support from the Research Grants Council of Hong Kong (No. 15304519), the National Natural Science Foundation of China (No. 11904306), and the Hong Kong Polytechnic University (No. 1-ZVH9). The authors also thank the Fundamental Research Funds for the Central Universities (Nos. 2019B02414 and 2019B44214) and PAPD, and Open Foundation of Key Laboratory of Industrial Ecology and Environmental Engineering, MOE (No. KLIEEE-18-02). The authors thank Dr. Romana Schirhagl and Miss Chuyi Xie for their careful proofreading of this article.

References

[1] Wang, L.; Zhang, Y.; Chen, L.; Xu, H. X.; Xiong, Y. J. 2D polymers as emerging materials for photocatalytic overall water splitting. *Adv. Mater.* **2018**, *30*, 1801955.

[2] Wasielewski, M. R. Self-assembly strategies for integrating light harvesting and charge separation in artificial photosynthetic systems. *Acc. Chem. Res.* **2009**, *42*, 1910–1921.

[3] Mora, S. J.; Odella, E.; Moore, G. F.; Gust, D.; Moore, T. A.; Moore, A. L. Proton-coupled electron transfer in artificial photosynthetic systems. *Acc. Chem. Res.* **2018**, *51*, 445–453.

[4] Rahman, M. Z.; Davey, K.; Qiao, S. Z. Carbon, nitrogen and phosphorus containing metal-free photocatalysts for hydrogen production: Progress and challenges. *J. Mater. Chem. A* **2018**, *6*, 1305–1322.

[5] Gan, X. R.; Lei, D. Y.; Wong, K. Y. Two-dimensional layered nanomaterials for visible-light-driven photocatalytic water splitting. *Mater. Today Energy* **2018**, *10*, 352–367.

[6] Weng, B.; Qi, M. Y.; Han, C.; Tang, Z. R.; Xu, Y. J. Photocorrosion inhibition of semiconductor-based photocatalysts: Basic principle, current development, and future perspective. *ACS Catal.* **2019**, *9*, 4642–4687.

[7] Bai, S.; Wang, L. L.; Li, Z. Q.; Xiong, Y. J. Facet-engineered surface and interface design of photocatalytic materials. *Adv. Sci.* **2017**, *4*, 1600216.

[8] Hu, Y. G.; Gao, C.; Xiong, Y. J. Surface and interface design for photocatalytic water splitting. *Dalton Trans.* **2018**, *47*, 12035–12040.

[9] Wang, H. L.; Zhang, L. S.; Chen, Z. G.; Hu, J. Q.; Li, S. J.; Wang, Z. H.; Liu, J. S.; Wang, X. C. Semiconductor heterojunction photocatalysts: Design, construction, and photocatalytic performances. *Chem. Soc. Rev.* **2014**, *43*, 5234–5244.

[10] Xia, F. N.; Wang, H.; Xiao, D.; Dubey, M.; Ramasubramaniam, A. Two-dimensional material nanophotonics. *Nat. Photonics* **2014**, *8*, 899–907.

[11] Zhao, Y. F.; Jia, X. D.; Waterhouse, G. I. N.; Wu, L. Z.; Tung, C. H.; O'Hare, D.; Zhang, T. R. Layered double hydroxide nanostructured photocatalysts for renewable energy production. *Adv. Energy Mater.* **2016**, *6*, 1501974.

[12] Zhao, Y. F.; Waterhouse, G. I. N.; Chen, G. B.; Xiong, X. Y.; Wu, L. Z.; Tung, C. H.; Zhang, T. R. Two-dimensional-related catalytic materials for solar-driven conversion of CO_x into valuable chemical feedstocks. *Chem. Soc. Rev.* **2019**, *48*, 1972–2010.

[13] Zhao, Y. X.; Zhang, S.; Shi, R.; Waterhouse, G. I. N.; Tang, J. W.; Zhang, T. R. Two-dimensional photocatalyst design: A critical review of recent experimental and computational advances. *Mater. Today* **2020**, *34*, 78–91.

[14] Ran, J. R.; Qu, J. T.; Zhang, H. P.; Wen, T.; Wang, H. L.; Chen, S. M.; Song, L.; Zhang, X. L.; Jing, L. Q.; Zheng, R. K. et al. 2D metal organic framework nanosheet: A universal platform promoting highly efficient visible-light-induced hydrogen production. *Adv. Energy Mater.* **2019**, *9*, 1803402.

[15] Xia, B. Q.; Ran, J. R.; Chen, S. M.; Song, L.; Zhang, X. L.; Jing, L. Q.; Qiao, S. Z. A two-dimensional metal-organic framework accelerating visible-light-driven H_2 production. *Nanoscale* **2019**, *11*, 8304–8309.

[16] Ran, J. R.; Zhu, B. C.; Qiao, S. Z. Phosphorene Co-catalyst advancing highly efficient visible-light photocatalytic hydrogen production. *Angew. Chem., Int. Ed.* **2017**, *56*, 10373–10377.
[17] Tan, C. L.; Lai, Z. C.; Zhang, H. Ultrathin two-dimensional multinary layered metal chalcogenide nanomaterials. *Adv Mater* **2017**, *29*, 1701392.
[18] Yin, H. J.; Tang, Z. Y. Ultrathin two-dimensional layered metal hydroxides: An emerging platform for advanced catalysis, energy conversion and storage. *Chem. Soc. Rev.* **2016**, *45*, 4873–4891.
[19] Wang, H.; Zhang, X. D.; Xie, Y. Recent progress in ultrathin two-dimensional semiconductors for photocatalysis. *Mater. Sci. Eng. R Rep* **2018**, *130*, 1–39.
[20] Ida, S.; Ishihara, T. Recent progress in two-dimensional oxide photocatalysts for water splitting. *J. Phys. Chem. Lett.* **2014**, *5*, 2533–2542.
[21] Gan, X. R; Lee, L. Y. S.; Wong, K. Y.; Lo, T. W.; Ho, K. H.; Lei, D. Y.; Zhao, H. M. 2H/1T phase transition of multilayer MoS_2 by electrochemical incorporation of s vacancies. *ACS Appl. Energy Mater.* **2018**, *1*, 4754–4765.
[22] Sun, X.; Deng, H. T.; Zhu, W. G.; Yu, Z.; Wu, C. Z.; Xie, Y. Interface engineering in two-dimensional heterostructures: Towards an advanced catalyst for Ullmann couplings. *Angew. Chem., Int. Ed.* **2016**, *55*, 1704–1709.
[23] Choi, W.; Choudhary, N.; Han, G. H.; Park, J.; Akinwande, D.; Lee, Y. H. Recent development of two-dimensional transition metal dichalcogenides and their applications. *Mater. Today* **2017**, *20*, 116–130.
[24] Lv, R. T.; Robinson, J. A.; Schaak, R. E.; Sun, D.; Sun, Y. F.; Mallouk, T. E.; Terrones, M. Transition metal dichalcogenides and beyond: Synthesis, properties, and applications of single- and few-layer nanosheets. *Acc. Chem. Res.* **2015**, *48*, 56–64.
[25] Su, T. M.; Shao, Q.; Qin, Z. Z.; Guo, Z. H.; Wu, Z. L. Role of interfaces in two-dimensional photocatalyst for water splitting. *ACS Catal.* **2018**, *8*, 2253–2276.
[26] Rahmanian, E.; Malekfar, R.; Pumera, M. Nanohybrids of two-dimensional transition-metal dichalcogenides and titanium dioxide for photocatalytic applications. *Chem.—Eur. J.* **2018**, *24*, 18–31.
[27] Wang, F. M.; Shifa, T. A.; Zhan, X. Y.; Huang, Y.; Liu, K. L.; Cheng, Z. Z.; Jiang, C.; He, J. Recent advances in transition-metal dichalcogenide based nanomaterials for water splitting. *Nanoscale* **2015**, *7*, 19764–19788.
[28] Zhong, Y. Y.; Zhao, G.; Ma, F. K.; Wu, Y. Z.; Hao, X. P. Utilizing photocorrosion-recrystallization to prepare a highly stable and efficient CdS/WS_2 nanocomposite photocatalyst for hydrogen evolution. *Appl. Catal. B Environ.* **2016**, *199*, 466–472.
[29] Yang, W. L.; Zhang, X. D.; Xie, Y. Advances and challenges in chemistry of two-dimensional nanosheets. *Nano Today* **2016**, *11*, 793–816.
[30] Lei, S. D.; Wang, X. F.; Li, B.; Kang, J. H.; He, Y. M.; George, A.; Ge, L. H.; Gong, Y. J.; Dong, P.; Jin, Z. H. et al. Surface functionalization of two-dimensional metal chalcogenides by Lewis acid-base chemistry. *Nat. Nanotechnol.* **2016**, *11*, 465–471.
[31] Guo, Y. Q.; Xu, K.; Wu, C. Z.; Zhao, J. Y.; Xie, Y. Surface chemical-modification for engineering the intrinsic physical properties of inorganic two-dimensional nanomaterials. *Chem. Soc. Rev.* **2015**, *44*, 637–646.
[32] Presolski, S.; Pumera, M. Covalent functionalization of MoS_2. *Mater. Today* **2016**, *19*, 140–145.
[33] Voiry, D.; Goswami, A.; Kappera, R.; Silva, C. D. C. C. E.; Kaplan, D.; Fujita, T.; Chen, M.; Asefa, T.; Chhowalla, M. Covalent functionalization of monolayered transition metal dichalcogenides by phase engineering. *Nat. Chem.* **2015**, *7*, 45–49.
[34] Gan, X. R.; Zhao, H. M.; Wong, K. Y.; Lei, D. Y.; Zhang, Y. B.; Quan, X. Covalent functionalization of MoS_2 nanosheets synthesized by liquid phase exfoliation to construct electrochemical sensors for Cd (II) detection. *Talanta* **2018**, *182*, 38–48.
[35] Vera-Hidalgo, M.; Giovanelli, E.; Navío, C.; Pérez, E. M. Mild covalent functionalization of transition metal dichalcogenides with maleimides: A "click" reaction for 2H-MoS_2 and WS_2. *J. Am. Chem. Soc.* **2019**, *141*, 3767–3771.
[36] Sumesh, C. K.; Peter, S. C. Two-dimensional semiconductor transition metal based chalcogenide based heterostructures for water splitting applications. *Dalton Trans.* **2019**, *48*, 12772–12802.
[37] Tiwari, A. P.; Novak, T. G.; Bu, X. M.; Ho, J. C.; Jeon, S. Layered ternary and quaternary transition metal chalcogenide based catalysts for water splitting. *Catalysts* **2018**, *8*, 551.
[38] Haque, F.; Daeneke, T.; Kalantar-zadeh, K.; Ou, J. Z. Two-dimensional transition metal oxide and chalcogenide-based photocatalysts. *Nano-Micro Lett.* **2018**, *10*, 23.
[39] Li, H. N.; Shi, Y. M.; Chiu, M. H.; Li, L. J. Emerging energy applications of two-dimensional layered transition metal dichalcogenides. *Nano Energy* **2015**, *18*, 293–305.
[40] Zhang, X.; Lai, Z. C.; Ma, Q. L.; Zhang, H. Novel structured transition metal dichalcogenide nanosheets. *Chem. Soc. Rev.* **2018**, *47*, 3301–3338.
[41] Chen, Y.; Fan, Z. X.; Zhang, Z.C.; Niu, W. X.; Li, C. L.; Yang, N. L.; Chen, B.; Zhang, H. Two-dimensional metal nanomaterials: Synthesis, properties, and applications. *Chem. Rev.* **2018**, *118*, 6409–6455.
[42] Tan, C. L.; Zhang, H. Two-dimensional transition metal dichalcogenide nanosheet-based composites. *Chem. Soc. Rev.* **2015**, *44*, 2713–2731.
[43] Manzeli, S.; Ovchinnikov, D.; Pasquier, D.; Yazyev, O. V.; Kis, A. 2D transition metal dichalcogenides. *Nat. Rev. Mater.* **2017**, *2*, 17033.
[44] Iwase, A.; Ng, Y. H.; Ishiguro, Y.; Kudo, A.; Amal, R. Reduced graphene oxide as a solid-state electron mediator in Z-scheme photocatalytic water splitting under visible light. *J. Am. Chem. Soc.* **2011**, *133*, 11054–11057.
[45] Kudo, A.; Miseki, Y. Heterogeneous photocatalyst materials for water splitting. *Chem. Soc. Rev.* **2009**, *38*, 253–278.
[46] Wang, Q.; Domen, K. Particulate photocatalysts for light-driven water splitting: Mechanisms, challenges, and design strategies. *Chem. Rev.* **2020**, *120*, 919–985.
[47] Sun, Z. P.; Martinez, A.; Wang, F. Optical modulators with 2D layered materials. *Nat. Photonics* **2016**, *10*, 227–238.
[48] Zhu, L. X.; Liu, F. Y.; Lin, H. T.; Hu, J. J.; Yu, Z. F.; Wang, X. R.; Fan, S. H. Angle-selective perfect absorption with two-dimensional materials. *Light Sci. Appl.* **2016**, *5*, e16052.
[49] Radisavljevic, B.; Kis, A. Mobility engineering and a metal-insulator transition in monolayer MoS_2. *Nat. Mater.* **2013**, *12*, 815–820.
[50] Zhou, S. Y.; Gweon, G. H.; Fedorov, A. V.; First, P. N.; De Heer, W. A.; Lee, D. H.; Guinea, F.; Neto, A. H. C.; Lanzara, A. Erratum: Substrate-induced bandgap opening in epitaxial graphene. *Nat. Mater.* **2007**, *6*, 916.
[51] Chen, X. B.; Shen, S. H.; Guo, L. J.; Mao, S. S. Semiconductor-based photocatalytic hydrogen generation. *Chem. Rev.* **2010**, *110*, 6503–6570.
[52] Nocera, D. G. The artificial leaf. *Acc. Chem. Res.* **2012**, *45*, 767–776.
[53] Sun, Y. F.; Gao, S.; Lei, F. C.; Xie, Y. Atomically-thin two-dimensional sheets for understanding active sites in catalysis. *Chem. Soc. Rev.* **2015**, *44*, 623–636.
[54] Jo, Y. K.; Lee, J. M.; Son, S.; Hwang, S. J. 2D inorganic nanosheet-based hybrid photocatalysts: Design, applications, and perspectives. *J. Photochem. Photobiol. C Photochem. Rev.* **2019**, *40*, 150–190.
[55] Yuan, Y. P.; Ruan, L. W.; Barber, J.; Loo, S. C. J.; Xue, C. Hetero-nanostructured suspended photocatalysts for solar-to-fuel conversion. *Energy. Environ. Sci.* **2014**, *7*, 3934–3951.
[56] Tong, H.; Ouyang, S. X.; Bi, Y. P.; Umezawa, N.; Oshikiri, M.; Ye, J. H. Nano-photocatalytic materials: Possibilities and challenges. *Adv. Mater.* **2012**, *24*, 229–251.
[57] Shao, N.; Wang, J. N.; Wang, D. D.; Corvini, P. Preparation of three-dimensional $Ag_3PO_4/TiO_2@MoS_2$ for enhanced visible-light photocatalytic activity and anti-photocorrosion. *Appl. Catal. B Environ.* **2017**, *203*, 964–978.
[58] Tian, S. F.; Chen, S. D.; Ren, X. T.; Cao, R. H.; Hu, H. Y.; Bai F. Bottom-up fabrication of graphitic carbon nitride nanosheets modified with porphyrin via covalent bonding for photocatalytic H_2 evolution. *Nano Res.* **2019**, *12*, 3109–3115.
[59] Zhou, P.; Yu, J. G.; Jaroniec, M. All-solid-state Z-scheme photocatalytic systems. *Adv. Mater.* **2014**, *26*, 4920–4935.
[60] Zheng, B. Y.; Ma, C.; Li, D.; Lan, J. Y.; Zhang, Z.; Sun, X. X.; Zheng, W. H.; Yang, T. F.; Zhu, C. G.; Ouyang, G. et al. Band alignment engineering in two-dimensional lateral heterostructures. *J. Am. Chem. Soc.* **2018**, *140*, 11193–11197.
[61] Zhang, J.; Qiao, S. Z.; Qi, L. F.; Yu, J. G. Fabrication of NiS modified CdS nanorod p-n junction photocatalysts with enhanced

visible-light photocatalytic H_2-production activity. *Phys. Chem. Chem. Phys.* **2013**, *15*, 12088–12094.
[62] Liu, Y.; Yu, Y. X.; Zhang, W. D. MoS_2/CdS heterojunction with high photoelectrochemical activity for H_2 evolution under visible light: The role of MoS_2. *J. Phys. Chem. C* **2013**, *117*, 12949–12957.
[63] Mushtaq, A.; Ghosh, S.; Sarkar, A. S.; Pal, S. K. Multiple exciton harvesting at zero-dimensional/two-dimensional heterostructures. *ACS Energy Lett.* **2017**, *2*, 1879–1885.
[64] Xu, Q. L.; Zhang, L. Y.; Yu, J. G.; Wageh, S.; Al-Ghamdi, A. A.; Jaroniec, M. Direct Z-scheme photocatalysts: Principles, synthesis, and applications. *Mater. Today* **2018**, *21*, 1042–1063.
[65] Li, X. G.; Bi, W. T.; Zhang, L.; Tao, S.; Chu, W. S.; Zhang, Q.; Luo, Y.; Wu, C. Z.; Xie, Y. Single-atom Pt as co-catalyst for enhanced photocatalytic H_2 evolution. *Adv. Mater.* **2016**, *28*, 2427–2431.
[66] Ma, X. Y.; Li, J. Q.; An, C. H.; Feng, J.; Chi, Y. H.; Liu, J. X.; Zhang, J.; Sun, Y. G. Ultrathin Co(Ni)-doped MoS_2 nanosheets as catalytic promoters enabling efficient solar hydrogen production. *Nano Res.* **2016**, *9*, 2284–2293.
[67] Radisavljevic, B.; Radenovic, A.; Brivio, J.; Giacometti, V.; Kis, A. Single-layer MoS_2 transistors. *Nat. Nanotechnol.* **2011**, *6*, 147–150.
[68] Gu, Q.; Sun, H. M.; Xie, Z. Y.; Gao, Z. W.; Xue, C. MoS_2-coated microspheres of self-sensitized carbon nitride for efficient photocatalytic hydrogen generation under visible light irradiation. *Appl. Surf. Sci.* **2017**, *396*, 1808–1815.
[69] Di, J.; Yan, C.; Handoko, A. D.; Seh, Z. W.; Li, H. M.; Liu, Z. Ultrathin two-dimensional materials for photo- and electrocatalytic hydrogen evolution. *Mater. Today* **2018**, *21*, 749–770.
[70] Di, J.; Xiong, J.; Li, H. M.; Liu, Z. Ultrathin 2D photocatalysts: Electronic-structure tailoring, hybridization, and applications. *Adv. Mater.* **2018**, *30*, 1704548.
[71] Low, J. X.; Yu, J. G.; Jaroniec, M.; Wageh, S.; Al-Ghamdi, A. A. Heterojunction photocatalysts. *Adv. Mater.* **2017**, *29*, 1601694.
[72] Luo, B.; Liu, G.; Wang, L. Z. Recent advances in 2D materials for photocatalysis. *Nanoscale* **2016**, *8*, 6904–6920.
[73] Ran, J. R.; Jaroniec, M.; Qiao, S. Z. Cocatalysts in semiconductor-based photocatalytic CO_2 reduction: Achievements, challenges, and opportunities. *Adv. Mater.* **2018**, *30*, 1704649.
[74] Shiraishi, Y.; Kofuji, Y.; Kanazawa, S.; Sakamoto, H.; Ichikawa, S.; Tanaka, S.; Hirai, T. Platinum nanoparticles strongly associated with graphitic carbon nitride as efficient co-catalysts for photocatalytic hydrogen evolution under visible light. *Chem. Commun.* **2014**, *50*, 15255–15258.
[75] Zhang, J.; Zhu, Z. P.; Tang, Y. P.; Müllen, K.; Feng, X. L. Titania nanosheet-mediated construction of a two-dimensional titania/cadmium sulfide heterostructure for high hydrogen evolution activity. *Adv. Mater.* **2014**, *26*, 734–738.
[76] Bi, W. T.; Li, X. G.; Zhang, L.; Jin, T.; Zhang, L. D.; Zhang, Q.; Luo, Y.; Wu, C. Z.; Xie, Y. Molecular co-catalyst accelerating hole transfer for enhanced photocatalytic H_2 evolution. *Nat. Commun.* **2015**, *6*, 8647.
[77] Jin, Y.; Jiang, D. L.; Li, D.; Xiao, P.; Ma, X. D.; Chen, M. $SrTiO_3$ nanoparticle/$SnNb_2O_6$ nanosheet 0D/2D heterojunctions with enhanced interfacial charge separation and photocatalytic hydrogen evolution activity. *ACS Sustainable Chem. Eng.* **2017**, *5*, 9749–9757.
[78] Tan, L.; Li, P. D.; Sun, B. Q.; Chaker, M.; Ma, D. L. Stabilities related to near-infrared quantum dot-based solar cells: The role of surface engineering. *ACS Energy Lett.* **2017**, *2*, 1573–1585.
[79] Pincella, F.; Isozaki, K.; Miki, K. A visible light-driven plasmonic photocatalyst. *Light Sci. Appl.* **2014**, *3*, e133.
[80] Chen, W.; Zhang, S. P.; Kang, M.; Liu, W. K.; Ou, Z. W.; Li, Y.; Zhang, Y. X.; Guan, Z. Q.; Xu, H. X. Probing the limits of plasmonic enhancement using a two-dimensional atomic crystal probe. *Light Sci. Appl.* **2018**, *7*, 56.
[81] Ma, X. C.; Dai, Y.; Yu, L.; Huang, B. B. Energy transfer in plasmonic photocatalytic composites. *Light Sci. Appl.* **2016**, *5*, e16017.
[82] Tian, Y.; Tatsuma, T. Mechanisms and applications of plasmon-induced charge separation at TiO_2 films loaded with gold nanoparticles. *J. Am. Chem. Soc.* **2005**, *127*, 7632–7637.
[83] Shan, H. Y.; Yu, Y.; Wang, X. L.; Luo, Y.; Zu, S.; Du, B. W.; Han, T. Y.; Li, B. W.; Li, Y.; Wu, J. R. et al. Direct observation of ultrafast plasmonic hot electron transfer in the strong coupling regime. *Light Sci. Appl.* **2019**, *8*, 9.
[84] Zhang, F.; Zhuang, H. Q.; Song, J.; Men, Y. L.; Pan, Y. X.; Yu, S. H. Coupling cobalt sulfide nanosheets with cadmium sulfide nanoparticles for highly efficient visible-light-driven photocatalysis. *Appl. Catal. B Environ.* **2018**, *226*, 103–110.
[85] Zhang, Z.; Yates, Jr. J. T. Band bending in semiconductors: Chemical and physical consequences at surfaces and interfaces. *Chem. Rev.* **2012**, *112*, 5520–5551.
[86] Maeda, K.; Teramura, K.; Lu, D. L.; Saito, N.; Inoue, Y.; Domen, K. Noble-metal/Cr_2O_3 core/shell nanoparticles as a cocatalyst for photocatalytic overall water splitting. *Angew. Chem., Int., Ed.* **2006**, *45*, 7806–7809.
[87] Garcia-Esparza, A. T.; Shinagawa, T.; Ould-Chikh, S.; Qureshi, M.; Peng, X. Y.; Wei, N. N.; Anjum, D. H.; Clo, A.; Weng, T. C.; Nordlund, D. et al. An oxygen-insensitive hydrogen evolution catalyst coated by a molybdenum-based layer for overall water splitting. *Angew. Chem., Int. Ed.* **2017**, *56*, 5780–5784.
[88] Bau, J. A.; Takanabe, K. Ultrathin microporous SiO_2 membranes photodeposited on hydrogen evolving catalysts enabling overall water splitting. *ACS Catal.* **2017**, *7*, 7931–7940.
[89] Xu, B.; He, P. L.; Liu, H. L.; Wang, P. P.; Zhou, G.; Wang, X. A 1D/2D helical CdS/$ZnIn_2S_4$ nano-heterostructure. *Angew. Chem., Int. Ed.* **2014**, *53*, 2339–2343.
[90] Liu, S. Q.; Tang, Z. R.; Sun, Y. G.; Colmenares, J. C.; Xu, Y. J. One-dimension-based spatially ordered architectures for solar energy conversion. *Chem. Soc. Rev.* **2015**, *44*, 5053–5075.
[91] Meng, F. K.; Li, J. T.; Cushing, S. K.; Bright, J.; Zhi, M. J.; Rowley, J. D.; Hong, Z. L.; Manivannan, A.; Bristow, A. D.; Wu, N. Q. Photocatalytic water oxidation by hematite/reduced graphene oxide composites. *ACS Catal.* **2013**, *3*, 746–751.
[92] Li, C.; Yu, Y. F.; Chi, M. F.; Cao, L. Y. Epitaxial nanosheet-nanowire heterostructures. *Nano Lett.* **2013**, *13*, 948–953.
[93] Zhang, X.; Chen, Y. J.; Xiao, Y. T.; Zhou, W.; Tian, G. H.; Fu, H. G. Enhanced charge transfer and separation of hierarchical hydrogenated TiO_2 nanothorns/carbon nanofibers composites decorated by NiS quantum dots for remarkable photocatalytic H_2 production activity. *Nanoscale* **2018**, *10*, 4041–4050.
[94] Zhang, X. C.; Hu, W. Y.; Zhang, K. F.; Wang, J. N.; Sun, B. J.; Li, H. Z.; Qiao, P. Z.; Wang, L.; Zhou, W. Ti^{3+} self-doped black TiO_2 nanotubes with mesoporous nanosheet architecture as efficient solar-driven hydrogen evolution photocatalysts. *ACS Sustainable Chem. Eng.* **2017**, *5*, 6894–6901.
[95] Zhou, B. H.; Yang, S. L.; Wu, W.; Sun, L. L.; Lei, M.; Pan, J.; Xiong, X. Self-assemble SnO_2@TiO_2 porous nanowire-nanosheet heterostructures for enhanced photocatalytic property. *CrystEngComm.* **2014**, *16*, 10863–10869.
[96] Li, H. B.; Xiao, J. P.; Fu, Q.; Bao, X. H. Confined catalysis under two-dimensional materials. *Proc. Natl. Acad. Sci. USA* **2017**, *114*, 5930–5934.
[97] Fu, Q.; Bao, X. H. Surface chemistry and catalysis confined under two-dimensional materials. *Chem. Soc. Rev.* **2017**, *46*, 1842–1874.
[98] Yang, X. F.; Tian, L.; Zhao, X. L.; Tang, H.; Liu, Q. Q.; Li, G. S. Interfacial optimization of g-C_3N_4-based Z-scheme heterojunction toward synergistic enhancement of solar-driven photocatalytic oxygen evolution. *App. Catal. B Environ.* **2019**, *244*, 240–249.
[99] Maeda, K.; Domen, K. Photocatalytic water splitting: Recent progress and future challenges. *J. Phys. Chem. Lett.* **2010**, *1*, 2655–2661.
[100] Gu, W. L.; Lu, F. X.; Wang, C.; Kuga, S.; Wu, L. Z.; Huang, Y.; Wu, M. Face-to-face interfacial assembly of ultrathin g-C_3N_4 and anatase TiO_2 nanosheets for enhanced solar photocatalytic activity. *ACS Appl. Mater. Interfaces* **2017**, *9*, 28674–28684.
[101] Parzinger, E.; Miller, B.; Blaschke, B.; Garrido, J. A.; Ager, J. W.; Holleitner, A.; Wurstbauer, U. Photocatalytic stability of single- and few-layer MoS_2. *ACS Nano* **2015**, *9*, 11302–11309.
[102] Park, K. H.; Choi, J.; Kim, H. J.; Oh, D. H.; Ahn, J. R.; Son, S. U. Unstable single-layered colloidal TiS_2 nanodisks. *Small* **2008**, *4*, 945–950.
[103] Balendhran, S.; Deng, J. K.; Ou, J. Z.; Walia, S.; Scott, J.; Tang, J. S.; Wang, K. L.; Field, M. R.; Russo, S.; Zhuiykov, S. et al. Enhanced charge carrier mobility in two-dimensional high dielectric molybdenum oxide. *Adv. Mater.* **2013**, *25*, 109–114.
[104] Li, W. J.; Lin, Z. Y.; Yang, G. W. A 2D self-assembled MoS_2/$ZnIn_2S_4$ heterostructure for efficient photocatalytic hydrogen evolution.

Nanoscale **2017**, *9*, 18290–18298.
[105] Li, G. W; Blake, G. R.; Palstra, T. T. M. Vacancies in functional materials for clean energy storage and harvesting: The perfect imperfection. *Chem. Soc. Rev.* **2017**, *46*, 1693–1706.
[106] Long, J. L.; Chang, H. J.; Gu, Q.; Xu, J.; Fan, L. Z.; Wang, S. C.; Zhou, Y. G.; Wei, W.; Huang, L.; Wang, X. X. et al. Gold-plasmon enhanced solar-to-hydrogen conversion on the {001} facets of anatase TiO_2 nanosheets. *Energy Environ. Sci.* **2014**, *7*, 973–977.
[107] Wang, L. L.; Ge, J.; Wang, A. L.; Deng, M. S.; Wang, X. J.; Bai, S.; Li, R.; Jiang, J.; Zhang, Q.; Luo, Y. et al. Designing p-type semiconductor-metal hybrid structures for improved photocatalysis. *Angew. Chem., Int. Ed.* **2014**, *53*, 5107–5111.
[108] Ismail, A. A.; Bahnemann, D. W. Photochemical splitting of water for hydrogen production by photocatalysis: A review. *Solar Energy Mater. Solar Cells* **2014**, *128*, 85–101.
[109] Chen, J. H.; Bailey, C. S.; Hong, Y. L.; Wang, L.; Cai, Z.; Shen, L.; Hou, B. Y.; Wang, Y.; Shi, H. T.; Sambur, J. et al. Plasmon-resonant enhancement of photocatalysis on monolayer WSe_2. *ACS Photonics* **2019**, *6*, 787–792.
[110] Linic, S.; Christopher, P.; Ingram, D. B. Plasmonic-metal nanostructures for efficient conversion of solar to chemical energy. *Nat. Mater.* **2011**, *10*, 911–921.
[111] Choi, S. Y.; Yip, C. T.; Li, G. C.; Lei, D. Y.; Fung, K. H.; Yu, S. F.; Hao, J. H. Photoluminescence enhancement in few-layer WS_2 films via Au nanoparticles. *AIP Adv.* **2015**, *5*, 067148.
[112] Kang, T. D.; Yoon, J. G. Optical characterization of surface plasmon resonance of Pt nanoparticles in TiO_2-SiO_2 nanocomposite films. *J. Appl. Phys.* **2017**, *122*, 134302.
[113] Li, X. H.; Guo, S. H.; Kan, C. X.; Zhu, J. M.; Tong, T. T.; Ke, S. L.; Choy, W. C. H.; Wei, B. Q. Au multimer@MoS_2 hybrid structures for efficient photocatalytical hydrogen production via strongly plasmonic coupling effect. *Nano Energy* **2016**, *30*, 549–558.
[114] Zhang, N.; Han, C.; Xu, Y. J.; Foley IV, J. J.; Zhang, D. T.; Codrington, J.; Gray, S. K.; Sun, Y. G. Near-field dielectric scattering promotes optical absorption by platinum nanoparticles. *Nat. Photonics* **2016**, *10*, 473–482.
[115] Minguez-Bacho, I.; Courte, M.; Fan, H. J.; Fichou, D. Conformal Cu_2S-coated Cu_2O nanostructures grown by ion exchange reaction and their photoelectrochemical properties. *Nanotechnology* **2015**, *26*, 185401.
[116] Liu, Y.; Zhang, Z. Y.; Fang, Y. R.; Liu, B. K.; Huang, J. D.; Miao, F. J.; Bao, Y. A.; Dong, B. IR-driven strong plasmonic-coupling on Ag nanorices/$W_{18}O_{49}$ nanowires heterostructures for photo/thermal synergistic enhancement of H_2 evolution from ammonia borane. *Appl. Catal. B Environ.* **2019**, *252*, 164–173.
[117] Zhang, Y. Z.; Guo, S. H.; Xin, X.; Song, Y. R.; Yang, L.; Wang, B. L.; Tan, L. L.; Li, X. H. Plasmonic MoO_2 as co-catalyst of MoS_2 for enhanced photocatalytic hydrogen evolution. *Appl Surf. Sci.* **2020**, *504*, 144291.
[118] Guo, L.; Yang, Z.; Marcus, K.; Li, Z.; Luo, B.; Zhou, L.; Wang, X.; Du, Y.; Yang, Y. MoS_2/TiO_2 heterostructures as nonmetal plasmonic photocatalysts for highly efficient hydrogen evolution. *Energy Environ. Sci.* **2018**, *11*, 106–114.
[119] Chen, J. Z.; Wu, X. J.; Yin. L. S.; Li, B.; Hong, X.; Fan, Z. X.; Chen, B.; Xue, C.; Zhang, H. One-pot synthesis of CdS nanocrystals hybridized with single-layer transition-metal dichalcogenide nanosheets for efficient photocatalytic hydrogen evolution. *Angew. Chem., Int. Ed.* **2015**, *54*, 1210–1214.
[120] Zong, X.; Yan, H. J.; Wu, G. P.; Ma, G. J.; Wen, F. Y.; Wang, L.; Li, C. Enhancement of photocatalytic H_2 evolution on CdS by loading MoS_2 as cocatalyst under visible light irradiation. *J. Am. Chem. Soc.* **2008**, *130*, 7176–7177.
[121] Gan, X. R.; Zhao, H. M.; Quan, X. Two-dimensional MoS_2: A promising building block for biosensors. *Biosens. Bioelectron.* **2017**, *89*, 56–71.
[122] Li, D.; Liu, Y.; Shi, W. W.; Shao, C. Y.; Wang, S. Y.; Ding, C. M.; Liu, T. F.; Fan, F. T.; Shi, J. Y.; Li, C. Crystallographic-orientation-dependent charge separation of $BiVO_4$ for solar water oxidation. *ACS Energy Lett.* **2019**, *4*, 825–831.
[123] Yang, L.; Zhong, D.; Zhang, J. Y.; Yan, Z. P.; Ge, S. F.; Du, P. W.; Jiang, J.; Sun, D.; Wu, X. J.; Fan, Z. Y. et al. Optical properties of metal-molybdenum disulfide hybrid nanosheets and their application for enhanced photocatalytic hydrogen evolution. *ACS Nano* **2014**, *8*, 6979–6985.
[124] Wen, J. Q.; Xie, J.; Zhang, H. D.; Zhang, A. P.; Liu, Y. J.; Chen, X. B.; Li, X. Constructing multifunctional metallic Ni interface layers in the g-C_3N_4 nanosheets/amorphous NiS heterojunctions for efficient photocatalytic H_2 generation. *ACS Appl. Mater. Interfaces* **2017**, *9*, 14031–14042.
[125] Sun, S. C.; Zhang, Y. C.; Shen, G. Q.; Wang, Y. T.; Liu, X. L.; Duan, Z. W.; Pan, L.; Zhang, X. W.; Zou, J. J. Photoinduced composite of Pt decorated $Ni(OH)_2$ as strongly synergetic cocatalyst to boost H_2O activation for photocatalytic overall water splitting. *Appl. Catal. B Environ.* **2019**, *243*, 253–261.
[126] He, K. L.; Xie, J.; Yang Z. H., Shen R. C., Fang Y. P.; Ma, S.; Chen, X. B.; Li X. Earth-abundant WC nanoparticles as an active noble-metal-free co-catalyst for the highly boosted photocatalytic H_2 production over g-C_3N_4 nanosheets under visible light. *Catal. Sci. Technol.* **2017**, *7*, 1193–1202.
[127] Shen, R. C.; Xie, J.; Zhang, H. D.; Zhang, A. P.; Chen, X. B.; Li, X. Enhanced solar fuel H_2 generation over g-C_3N_4 nanosheet photocatalysts by the synergetic effect of noble metal-free Co_2P cocatalyst and the environmental phosphorylation strategy. *ACS Sustainable Chem. Eng.* **2018**, *6*, 816–826.
[128] Jiang, L. S.; Wang, K.; Wu, X. Y.; Zhang, G. K.; Yin, S. Amorphous bimetallic cobalt nickel sulfide cocatalysts for significantly boosting photocatalytic hydrogen evolution performance of graphitic carbon nitride: Efficient interfacial charge transfer. *ACS Appl. Mater. Interfaces* **2019**, *11*, 26898–26908.
[129] Zhang, S. Q.; Liu, X.; Liu, C. B.; Luo, S. L.; Wang, L. L.; Cai, T.; Zeng, Y. X.; Yuan, J. L.; Dong, W. Y.; Pei, Y. et al. MoS_2 quantum dot growth induced by S vacancies in a $ZnIn_2S_4$ monolayer: Atomic-level heterostructure for photocatalytic hydrogen production. *ACS Nano* **2018**, *12*, 751–758.
[130] Zhang, K; Lin, Y. X.; Muhammad, Z.; Wu, C. Q.; Yang, S.; He, Q.; Zheng, X. S.; Chen, S. M.; Ge, B. H.; Song, L. Active {010} facet-exposed Cu_2MoS_4 nanotube as high-efficiency photocatalyst. *Nano Res.* **2017**, *10*, 3817–3825.
[131] Li, M. Q.; Cui, Z.; Li, E. L. Silver-modified MoS_2 nanosheets as a high-efficiency visible-light photocatalyst for water splitting. *Ceram. Int.* **2019**, *45*, 14449–14456.
[132] Xiong, J. H,; Liu, Y. H.; Wang, D. K.; Liang, S. J.; Wu, W. M.; Wu, L. An efficient cocatalyst of defect-decorated MoS_2 ultrathin nanoplates for the promotion of photocatalytic hydrogen evolution over CdS nanocrystal. *J. Mater. Chem. A* **2015**, *3*, 12631–12635.
[133] Zhang, X. H.; Li, N.; Wu, J. J.; Zheng, Y. Z.; Tao, X. Defect-rich O-incorporated 1T-MoS_2 nanosheets for remarkably enhanced visible-light photocatalytic H_2 evolution over CdS: The impact of enriched defects. *Appl. Catal. B Environ.* **2018**, *229*, 227–236.
[134] Zhang, S. W.; Yang, H. C.; Gao, H. H.; Cao, R. Y.; Huang, J. Z.; Xu, X. J. One-pot synthesis of CdS irregular nanospheres hybridized with oxygen-incorporated defect-rich MoS_2 ultrathin nanosheets for efficient photocatalytic hydrogen evolution. *ACS Appl. Mater. Interfaces* **2017**, *9*, 23635–23646.
[135] Yeh, T. F.; Chen, S. J.; Teng, H. Synergistic effect of oxygen and nitrogen functionalities for graphene-based quantum dots used in photocatalytic H_2 production from water decomposition. *Nano Energy* **2015**, *12*, 476–485.
[136] Yeh, T. F.; Teng, C. Y.; Chen, S. J.; Teng, H. Nitrogen-doped graphene oxide quantum dots as photocatalysts for overall water-splitting under visible light illumination. *Adv. Mater.* **2014**, *26*, 3297–3303.
[137] Liu, F. L.; Huang, C.; Liu, C. X.; Shi, R.; Chen, Y. Black phosphorus-based semiconductor heterojunctions for photocatalytic water splitting. *Chem.—Eur. J.* **2020**, *26*, 4449–4460.
[138] Shearer, C. J.; Cherevan, A.; Eder, D. Application and future challenges of functional nanocarbon hybrids. *Adv. Mater.* **2014**, *26*, 2295–2318.
[139] Nguyen, B. S.; Xiao, Y. K.; Shih, C. Y.; Nguyen, V. C.; Chou, W. Y.; Teng, H. Electronic structure manipulation of graphene dots for effective hydrogen evolution from photocatalytic water decomposition. *Nanoscale* **2018**, *10*, 10721–10730.
[140] Mateo, D.; García-Mulero, A.; Albero, J.; García, H. N-doped defective graphene decorated by strontium titanate as efficient

photocatalyst for overall water splitting. *Appl. Catal. B Environ.* **2019**, *252*, 111–119.

[141] Xie, G. C; Guan, L. M.; Zhang, L. J.; Guo, B. D.; Batool, A.; Xin, Q.; Boddula, R.; Jan, S. U.; Gong, J. R. Interaction-dependent interfacial charge-transfer behavior in solar water-splitting systems. *Nano Lett.* **2019**, *19*, 1234–1241.

[142] Xia, Y.; Cheng, B.; Fan, J. J.; Yu, J. G.; Liu, G. Unraveling photoexcited charge transfer pathway and process of CdS/graphene nanoribbon composites toward visible-light photocatalytic hydrogen evolution. *Small* **2019**, *15*, 1902459.

[143] Chen, T. J.; Song, C. J.; Fan, M. S.; Hong, Y. Z.; Hu, B.; Yu, L. B.; Shi, W. D. *In-situ* fabrication of CuS/g-C_3N_4 nanocomposites with enhanced photocatalytic H_2-production activity via photoinduced interfacial charge transfer. *Int. J. Hydrogen Energy* **2017**, *42*, 12210–12219.

[144] Sui, Y. L.; Wu, L.; Zhong, S. K.; Liu, Q. X. Carbon quantum dots/TiO_2 nanosheets with dominant (001) facets for enhanced photocatalytic hydrogen evolution. *Appl. Surf. Sci.* **2019**, *480*, 810–816.

[145] Ratnayake, S. P.; Mantilaka, M. M. M. G. P. G.; Sandaruwan, C.; Dahanayake, D.; Murugan, E.; Kumar, S.; Amaratunga, G. A. J.; De Silva, K. M. N. Carbon quantum dots-decorated nano-zirconia: A highly efficient photocatalyst. *Appl. Catal. A Gen.* **2019**, *570*, 23–30.

[146] Ozel, F.; Aslan, E.; Istanbullu, B.; Akay, O.; Patir, I. H. Photocatalytic hydrogen evolution based on Cu_2ZnSnS_4, Cu_2NiSnS_4 and Cu_2CoSnS_4 nanocrystals. *Appl. Catal. B Environ.* **2016**, *198*, 67–73.

[147] Hu, Y. D.; Chen, G.; Li, C. M.; Zhou, Y. S.; Sun, J. X.; Hao, S.; Han, Z. H. Fabrication of {010} facet dominant $BiTaO_4$ single-crystal nanoplates for efficient photocatalytic performance. *J. Mater. Chem. A* **2016**, *4*, 5274–5281.

[148] Chen, W. Z.; Hou, X. H.; Shi, X. Q.; Pan, H. Two-dimensional Janus transition metal oxides and chalcogenides: Multifunctional properties for photocatalysts, electronics, and energy conversion. *ACS Appl. Mater. Interfaces* **2018**, *10*, 35289–35295.

[149] Zhang, J.; Jia, S.; Kholmanov, I.; Dong, L.; Er, D. Q.; Chen, W. B.; Guo, H.; Jin, Z. H.; Shenoy, V. B.; Shi, L. et al. Janus monolayer transition-metal dichalcogenides. *ACS Nano* **2017**, *11*, 8192–8198.

[150] Wang, L.; Zhou, H. H.; Zhang, H. Z.; Song, Y. L.; Zhang, H.; Qian, X. H. SiO_2@TiO_2 core@shell nanoparticles deposited on 2D-layered $ZnIn_2S_4$ to form a ternary heterostructure for simultaneous photocatalytic hydrogen production and organic pollutant degradation. *Inorg. Chem.* **2020**, *59*, 2278–2287.

[151] Wang, B.; Cai, H. R.; Shen, S. H. Single metal atom photocatalysis. *Small Methods* **2019**, *3*, 1800447.

[152] Wang, Y.; Zhang, W. H.; Deng, D. H.; Bao, X. H. Two-dimensional materials confining single atoms for catalysis. *Chin. J. Catal.* **2017**, *38*, 1443–1453.

[153] Gao, C.; Low, J. X.; Long, R.; Kong, T. T.; Zhu, J. F.; Xiong, Y. J. Heterogeneous single-atom photocatalysts: Fundamentals and applications. *Chem. Rev.*, in press, https://doi.org/10.1021/acs.chemrev.9b00840.

[154] Shoaib, A.; Ji, M. W.; Qian, H. M.; Liu, J. J.; Xu, M.; Zhang, J. T. Noble metal nanoclusters and their *in situ* calcination to nanocrystals: Precise control of their size and interface with TiO_2 nanosheets and their versatile catalysis applications. *Nano Res.* **2016**, *9*, 1763–1774.

[155] Chen, S. S.; Takata, T.; Domen, K. Particulate photocatalysts for overall water splitting. *Nat. Rev. Mater.* **2017**, *2*, 17050.

[156] He, T. W.; Zhang, C. M.; Zhang, L.; Du, A. J. Single Pt atom decorated graphitic carbon nitride as an efficient photocatalyst for the hydrogenation of nitrobenzene into aniline. *Nano Res.* **2019**, *12*, 1817–1823.

[157] Fang, X. Z.; Shang, Q. C.; Wang, Y.; Jiao, L.; Yao, T.; Li, Y. F.; Zhang, Q.; Luo, Y.; Jiang, H. L. Single Pt atoms confined into a metal-organic framework for efficient photocatalysis. *Adv. Mater.* **2018**, *30*, 1705112.

[158] Cao, Y. J.; Wang, D. H.; Lin, Y.; Liu, W.; Cao, L. L.; Liu, X. K.; Zhang, W.; Mou, X. L.; Fang, S.; Shen, X. Y. et al. Single Pt atom with highly vacant d-orbital for accelerating photocatalytic H_2 evolution. *ACS Appl. Energy Mater.* **2018**, *1*, 6082–6088.

[159] Su, H.; Che, W.; Tang, F. M.; Cheng, W. R.; Zhao, X.; Zhang, H.; Liu, Q. H. Valence band engineering via Pt^{II} single-atom confinement realizing photocatalytic water splitting. *J. Phys. Chem. C* **2018**, *122*, 21108–21114.

[160] Zhao, Q.; Sun, J.; Li, S. C.; Huang, C. P.; Yao, W. F.; Chen, W.; Zeng, T.; Wu, Q.; Xu, Q. J. Single nickel atoms anchored on nitrogen-doped graphene as a highly active cocatalyst for photocatalytic H_2 evolution. *ACS Catal.* **2018**, *8*, 11863–11874.

[161] Zhao, Q.; Yao, W. F.; Huang, C. P.; Wu, Q.; Xu, Q. J. Effective and durable Co single atomic cocatalysts for photocatalytic hydrogen production. *ACS Appl. Mater. Interfaces* **2017**, *9*, 42734–42741.

[162] Zong, X.; Han, J. F.; Ma, G. J.; Yan, H. J.; Wu, G. P.; Li, C. Photocatalytic H_2 evolution on CdS loaded with WS_2 as cocatalyst under visible light irradiation. *J. Phys. Chem. C* **2011**, *115*, 12202–12208.

[163] Liu, X. F.; Xing, Z. P.; Zhang, H.; Wang, W. M.; Zhang, Y.; Li, Z. Z.; Wu, X. Y.; Yu, X. J.; Zhou, W. Fabrication of 3D mesoporous black TiO_2/MoS_2/TiO_2 nanosheets for visible-light-driven photocatalysis. *ChemSusChem* **2016**, *9*, 1118–1124.

[164] Shao, M. M.; Shao, Y. F.; Ding, S. J.; Tong, R.; Zhong, X. W.; Yao, L. M.; Ip, W. F.; Xu, B. M.; Shi, X. Q.; Sun, Y. Y. et al. Carbonized MoS_2: Super-active Co-catalyst for highly efficient water splitting on CdS. *ACS Sustainable Chem. Eng.* **2019**, *7*, 4220–4229.

[165] Xiong, M. H.; Chai, B.; Yan J. T., Fan G. Z., Song G. S. Few-layer WS_2 decorating $ZnIn_2S_4$ with markedly promoted charge separation and photocatalytic H_2 evolution activity. *Appl. Surf. Sci.* **2020**, *514*, 145965.

[166] Chen, J. H.; Tan, J.; Wu, G. X.; Zhang, X. J; Xu, F.; Lu, Y. Q. Tunable and enhanced light emission in hybrid WS_2-optical-fiber-nanowire structures. *Light: Sci. Appl.* **2019**, *8*, 8.

[167] Li, Y.; Wang, L. L.; Cai, T.; Zhang, S. Q.; Liu, Y. T.; Song, Y. Z.; Dong, X. R.; Hu, L. Glucose-assisted synthesize 1D/2D nearly vertical CdS/MoS_2 heterostructures for efficient photocatalytic hydrogen evolution. *Chem. Eng. J.* **2017**, *321*, 366–374.

[168] Shen, M.; Yan, Z. P.; Yang, L.; Du, P. W.; Zhang, J. Y.; Xiang, B. MoS_2 nanosheet/TiO_2 nanowire hybrid nanostructures for enhanced visible-light photocatalytic activities. *Chem. Commun.* **2014**, *50*, 15447–15449.

[169] Liu, C. B.; Wang, L. L.; Tang, Y. H.; Luo, S. L.; Liu, Y. T.; Zhang, S. Q.; Zeng, Y. X.; Xu, Y. Z. Vertical single or few-layer MoS_2 nanosheets rooting into TiO_2 nanofibers for highly efficient photocatalytic hydrogen evolution. *Appl. Catal. B Environ.* **2015**, *164*, 1–9.

[170] Chava, R. K.; Do, J. Y.; Kang, M. Hydrothermal growth of two dimensional hierarchical MoS_2 nanospheres on one dimensional CdS nanorods for high performance and stable visible photocatalytic H_2 evolution. *Appl. Surf. Sci.* **2018**, *433*, 240–248.

[171] Wang, T.; Chai, Y. Y.; Ma, D. K.; Chen, W.; Zheng, W. W.; Huang, S. M. Multidimensional CdS nanowire/$CdIn_2S_4$ nanosheet heterostructure for photocatalytic and photoelectrochemical applications. *Nano Res.* **2017**, *10*, 2699–2711.

[172] Feng, W. H.; Wang, Y. Z.; Huang, X. Y.; Wang, K. Q.; Gao, F.; Zhao, Y.; Wang, B.; Zhang, L. L.; Liu, P. One-pot construction of 1D/2D $Zn_{1-x}Cd_xS$/D-ZnS(en)$_{0.5}$ composites with perfect heterojunctions and their superior visible-light-driven photocatalytic H_2 evolution. *Appl. Catal. B Environ.* **2018**, *220*, 324–336.

[173] Li, H. D.; Wang, Y. N.; Chen, G. H.; Sang, Y. H.; Jiang, H. D.; He, J. T.; Li, X.; Liu, H. Few-layered MoS_2 nanosheets wrapped ultrafine TiO_2 nanobelts with enhanced photocatalytic property. *Nanoscale* **2016**, *8*, 6101–6109.

[174] Ma, B.; Guan, P. Y.; Li, Q. Y.; Zhang, M.; Zang, S. Q. MOF-derived flower-like MoS_2@TiO_2 nanohybrids with enhanced activity for hydrogen evolution. *ACS Appl. Mater. Inter.* **2016**, *8*, 26794–26800.

[175] Li, Q. H.; Qiao, X. Q.; Jia, Y. L.; Hou, D. F.; Li, D. S. Amorphous $CoMoS_4$ nanostructure for photocatalytic H_2 generation, nitrophenol reduction, and methylene blue adsorption. *ACS Appl. Nano Mater.* **2020**, *3*, 68–76.

[176] Xu, D. Y.; Xu, P. T.; Zhu, Y. Z.; Peng, W. C.; Li, Y.; Zhang, G. L.; Zhang, F. B.; Mallouk, T. E.; Fan, X. B. High yield exfoliation of WS_2 crystals into 1–2 layer semiconducting nanosheets and efficient photocatalytic hydrogen evolution from WS_2/CdS nanorod composites. *ACS Appl. Mater. Interfaces* **2018**, *10*, 2810–2818.

[177] Frisenda, R.; Molina-Mendoza, A. J.; Mueller, T.; Castellanos-Gomez, A.; van der Zant, H. S. J. Atomically thin p-n junctions based on two-dimensional materials. *Chem. Soc. Rev.* **2018**, *47*, 3339–3358.

[178] Li, D. S.; Wang, H. C.; Tang, H.; Yang, X. F.; Liu, Q. Q. Remarkable enhancement in solar oxygen evolution from $MoSe_2/Ag_3PO_4$ heterojunction photocatalyst via *in situ* constructing interfacial contact. *ACS Sustainable Chem. Eng.* **2019**, *7*, 8466–8474.

[179] Zhu, M. S.; Sun, Z. C.; Fujitsuka, M.; Majima, T. Z-scheme photocatalytic water splitting on a 2D heterostructure of black phosphorus/bismuth vanadate using visible light. *Angew. Chem., Int. Ed.* **2018**, *57*, 2160–2164.

[180] Pan, Z. M.; Zhang, G. G.; Wang, X. C. Polymeric carbon nitride/reduced graphene oxide/Fe_2O_3: All-solid-state Z-scheme system for photocatalytic overall water splitting. *Angew. Chem., Int. Ed.* **2019**, *58*, 7102–7106.

[181] Gao, G. H.; Gao, W.; Cannuccia, E.; Taha-Tijerina, J.; Balicas, L.; Mathkar, A.; Narayanan, T. N.; Liu, Z.; Gupta, B. K.; Peng, J. et al. Artificially stacked atomic layers: Toward new van der Waals solids. *Nano Lett.* **2012**, *12*, 3518–3525.

[182] Lin, Z.; McCreary, A.; Briggs, N.; Subramanian, S.; Zhang, K. H.; Sun, Y. F.; Li, X. F.; Borys, N. J.; Yuan, H. T.; Fullerton-Shirey, S. K. et al. 2D materials advances: From large scale synthesis and controlled heterostructures to improved characterization techniques, defects and applications. *2D Mater.* **2016**, *3*, 042001.

[183] Geim, A. K.; Grigorieva, I. V. van der Waals heterostructures. *Nature* **2013**, *499*, 419–425.

[184] Ou, Y.; Kang, Z.; Liao, Q. L.; Zhang, Z.; Zhang, Y. Edge induced band bending in van der Waals heterojunctions: A first principle study. *Nano Res.* **2020**, *13*, 701–708.

[185] Ma, S.; Xie, J.; Wen, J. Q.; He, K. L.; Li, X.; Liu, W.; Zhang, X. C. Constructing 2D layered hybrid CdS nanosheets/MoS_2 heterojunctions for enhanced visible-light photocatalytic H_2 generation. *Appl. Surf. Sci.* **2017**, *391*, 580–591.

[186] Meng, F. K.; Li, J. T.; Cushing, S. K.; Zhi, M. J.; Wu, N. Q. Solar hydrogen generation by nanoscale p-n junction of p-type molybdenum disulfide/n-type nitrogen-doped reduced graphene oxide. *J. Am. Chem. Soc.* **2013**, *135*, 10286–10289.

[187] Min, Y.; Im, E.; Hwang, G. T.; Kim, J. W.; Ahn, C. W.; Choi, J. J.; Hahn, B. D.; Choi, J. H.; Yoon, W. H.; Park, D. S. et al. Heterostructures in two-dimensional colloidal metal chalcogenides: Synthetic fundamentals and applications. *Nano Res.* **2019**, *12*, 1750–1769.

[188] Pu, C. C.; Wan, J.; Liu, E. Z.; Yin, Y. C.; Li, J.; Ma, Y. N.; Fan, J.; Hu, X. Y. Two-dimensional porous architecture of protonated GCN and reduced graphene oxide via electrostatic self-assembly strategy for high photocatalytic hydrogen evolution under visible light. *Appl. Surf. Sci.* **2017**, *399*, 139–150.

[189] Gong, Y. J.; Lin, J. H.; Wang, X. L.; Shi, G.; Lei, S. D.; Lin, Z.; Zou, X. L.; Ye, G. L.; Vajtai, R.; Yakobson, B. I. et al. Vertical and in-plane heterostructures from WS_2/MoS_2 monolayers. *Nat. Mater.* **2014**, *13*, 1135–1142.

[190] Yoon, Y.; Ganapathi, K.; Salahuddin, S. How good can monolayer MoS_2 transistors be? *Nano Lett.* **2011**, *11*, 3768–3773.

[191] Xu, J.; Zhang, J. J.; Zhang, W. J.; Lee, C. S. Interlayer nano-architectonics of two-dimensional transition-metal dichalcogenides nanosheets for energy storage and conversion applications. *Adv. Energy Mater.* **2017**, *7*, 1700571.

[192] Peng, R.; Liang, L. B.; Hood, Z. D.; Boulesbaa, A.; Puretzky, A.; Ievlev, A. V.; Come, J.; Ovchinnikova, O. S.; Wang, H.; Ma, C. et al. In-plane heterojunctions enable multiphasic two-dimensional (2D) MoS_2 nanosheets as efficient photocatalysts for hydrogen evolution from water reduction. *ACS Catal.* **2016**, *6*, 6723–6729.

[193] Yan, D. P.; Tang, Y. Q.; Lin, H. Y.; Wang, D. Tunable two-color luminescence and host-guest energy transfer of fluorescent chromophores encapsulated in metal-organic frameworks. *Sci. Rep.* **2015**, *4*, 4337.

[194] Putri, L. K.; Tan, L. L.; Ong, W. J.; Chang, W. S.; Chai, S. P. Graphene oxide: Exploiting its unique properties toward visible-light-driven photocatalysis. *Appl. Mater. Today* **2016**, *4*, 9–16.

[195] Thurston, T. R.; Wilcoxon, J. P. Photooxidation of organic chemicals catalyzed by nanoscale MoS_2. *J. Phys. Chem. B* **1999**, *103*, 11–17.

[196] Yuan, Y. J.; Tu, J. R.; Ye, Z. J.; Chen, D. Q.; Hu, B.; Huang, Y. W.; Chen, T. T.; Cao, D. P.; Yu, Z. T.; Zou, Z. G. MoS_2-graphene/$ZnIn_2S_4$ hierarchical microarchitectures with an electron transport bridge between light-harvesting semiconductor and cocatalyst: A highly efficient photocatalyst for solar hydrogen generation. *Appl. Catal. B Environ.* **2016**, *188*, 13–22.

[197] Yuan, Y. J.; Chen, D. Q.; Zhong, J. S.; Yang, L. X.; Wang, J. J.; Yu, Z. T.; Zou, Z. G. Construction of a noble-metal-free photocatalytic H_2 evolution system using MoS_2/reduced graphene oxide catalyst and zinc porphyrin photosensitizer. *J. Phys. Chem. C* **2017**, *121*, 24452–24462.

[198] Xia, P. F.; Zhu, B. C.; Cheng, B.; Yu, J. G.; Xu, J. S. 2D/2D g-C_3N_4/MnO_2 nanocomposite as a direct Z-scheme photocatalyst for enhanced photocatalytic activity. *ACS Sustainable Chem. Eng.* **2018**, *6*, 965–973.

[199] Yang, J. H.; Wang, D. E.; Han, H. X.; Li, C. Roles of cocatalysts in photocatalysis and photoelectrocatalysis. *Acc. Chem. Res.* **2013**, *46*, 1900–1909.

[200] Xu, J.; Zhang, J. J.; Zhang, W. J.; Lee, C. S. Interlayer nano-architectonics of two-dimensional transition-metal dichalcogenides nanosheets for energy storage and conversion applications. *Adv. Energy Mater.* **2017**, *7*, 1700571.

[201] Lu, N.; Guo, H. Y.; Wang, L.; Wu, X. J.; Zeng, X. C. van der Waals trilayers and superlattices: Modification of electronic structures of MoS_2 by intercalation. *Nanoscale* **2014**, *6*, 4566–4571.

[202] Wei, L.; Chen, Y. J.; Lin, Y. P.; Wu, H. S.; Yuan, R. S.; Li, Z. H. MoS_2 as non-noble-metal co-catalyst for photocatalytic hydrogen evolution over hexagonal $ZnIn_2S_4$ under visible light irradiations. *Appl. Catal. B Environ.* **2014**, *144*, 521–527.

[203] Yang, M. Q.; Xu, Y. J.; Lu, W. H.; Zeng, K. Y.; Zhu, H.; Xu, Q. H.; Ho, G. W. Self-surface charge exfoliation and electrostatically coordinated 2D hetero-layered hybrids. *Nat. Commun.* **2017**, *8*, 14224.

[204] Tan, P. F.; Zhu, A. Q.; Qiao, L. L.; Zeng, W. X.; Ma, Y. J.; Dong, H. G.; Xie, J. P.; Pan, J. Constructing a direct Z-scheme photocatalytic system based on 2D/2D $WO_3/ZnIn_2S_4$ nanocomposite for efficient hydrogen evolution under visible light. *Inorg. Chem. Front.* **2019**, *6*, 929–939.

[205] Iqbal, S.; Pan, Z. W.; Zhou, K. B. Enhanced photocatalytic hydrogen evolution from *in situ* formation of few-layered MoS_2/CdS nanosheet-based van der Waals heterostructures. *Nanoscale* **2017**, *9*, 6638–6642.

[206] Hou, Y. D.; Laursen, A. B.; Zhang, J. S.; Zhang, G. G.; Zhu, Y. S.; Wang, X. C.; Dahl, S.; Chorkendorff, I. Layered nanojunctions for hydrogen-evolution catalysis. *Angew. Chem., Int. Ed.* **2013**, *52*, 3621–3625.

[207] Lin, B.; Li, H.; An, H.; Hao, W. B.; Wei, J. J.; Dai, Y. Z.; Ma, C. S.; Yang, G. D. Preparation of 2D/2D g-C_3N_4 nanosheet@$ZnIn_2S_4$ nanoleaf heterojunctions with well-designed high-speed charge transfer nanochannels towards high-efficiency photocatalytic hydrogen evolution. *Appl. Catal. B Environ.* **2018**, *220*, 542–552.

[208] Li, J.; Zhan, G. M.; Yu, Y.; Zhang, L. Z. Superior visible light hydrogen evolution of Janus bilayer junctions via atomic-level charge flow steering. *Nat. Commun.* **2016**, *7*, 11480.

[209] Tian, G. H.; Chen, Y. J.; Ren, Z. Y.; Tian, C. G.; Pan, K.; Zhou, W.; Wang, J. Q.; Fu, H. G. Enhanced photocatalytic hydrogen evolution over hierarchical composites of $ZnIn_2S_4$ nanosheets grown on MoS_2 slices. *Chem.—Asian J.* **2014**, 9, 1291–1297.

[210] Li, Z. W.; Hou, J. G; Zhang, B.; Cao, S. Y.; Wu, Y. Z.; Gao, Z. M.; Nie, X. W.; Sun, L. C. Two-dimensional Janus heterostructures for superior Z-scheme photocatalytic water splitting. *Nano Energy* **2019**, *59*, 537–544.

[211] Zhu, C. Z.; Wang, Y. T.; Jiang, Z. F.; Xu, F. C.; Xian, Q. M.; Sun, C.; Tong, Q.; Zou, W. X.; Duan, X. G.; Wang, S. B. CeO_2 nanocrystal-modified layered MoS_2/g-C_3N_4 as 0D/2D ternary composite for visible-light photocatalytic hydrogen evolution: Interfacial consecutive multi-step electron transfer and enhanced H_2O reactant adsorption. *Appl. Catal. B Environ.* **2019**, *259*, 118072.

[212] Liu, D.; Zhang, S.; Wang, J. M.; Peng, T. Y.; Li, R. J. Direct Z-scheme 2D/2D photocatalyst based on ultrathin g-C_3N_4 and WO_3 nanosheets for efficient visible-light-driven H_2 generation. *ACS Appl. Mater. Interfaces* **2019**, *11*, 27913–27923.

[213] Lu, D. Z.; Wang, H. M.; Zhao, X. N.; Kondamareddy, K. K.; Ding, J. Q.; Li, C. H.; Fang, P. F. Highly efficient visible-light-induced photoactivity of Z-scheme g-C_3N_4/Ag/MoS_2 ternary photocatalysts for organic pollutant degradation and production of hydrogen. *ACS Sustainable Chem. Eng.* **2017**, *5*, 1436–1445.

[214] Chen, W.; Yan, R. Q.; Zhu, J. Q.; Huang, G. B.; Chen, Z. Highly efficient visible-light-driven photocatalytic hydrogen evolution by all-solid-state Z-scheme CdS/QDs/$ZnIn_2S_4$ architectures with MoS_2 quantum dots as solid-state electron mediator. *Appl. Surf. Sci.* **2020**, *504*, 144406.

[215] Ding, Y.; Wei, D. Q.; He, R.; Yuan, R. S.; Xie, T. F.; Li, Z. H. Rational design of Z-scheme PtS-$ZnIn_2S_4$/WO_3-MnO_2 for overall photo-catalytic water splitting under visible light. *Appl. Catal. B Environ.* **2019**, *258*, 117948.

[216] Maeda, K. Z-scheme water splitting using two different semiconductor photocatalysts. *ACS Catal.* **2013**, *3*, 1486–1503.

[217] Li, H. J.; Tu, W. G.; Zhou, Y.; Zou, Z. G. Z-scheme photocatalytic systems for promoting photocatalytic performance: Recent progress and future challenges. *Adv. Sci.* **2016**, *3*, 1500389.

[218] Yuan, Y. J.; Chen, D. Q.; Yang, S. H.; Yang, L. X.; Wang, J. J.; Cao, D. P.; Tu, W. G.; Yu, Z. T.; Zou, Z. G. Constructing noble-metal-free Z-scheme photocatalytic overall water splitting systems using MoS_2 nanosheet modified CdS as a H_2 evolution photocatalyst. *J. Mater. Chem. A* **2017**, *5*, 21205–21213.

[219] Lu, K. Q.; Qi, M. Y.; Tang, Z. R.; Xu, Y. J. Earth-abundant MoS_2 and cobalt phosphate dual cocatalysts on 1D CdS nanowires for boosting photocatalytic hydrogen production. *Langmuir* **2019**, *35*, 11056–11065.

[220] Tian, L.; Yang, X. F.; Cui, X. K.; Liu, Q. Q.; Tang, H. Fabrication of dual direct Z-scheme g-C_3N_4/MoS_2/Ag_3PO_4 photocatalyst and its oxygen evolution performance. *Appl. Surf. Sci.* **2019**, *463*, 9–17.

[221] Wang, Z. H.; Xu, X. J.; Si, Z. C.; Liu, L. P.; Liu, Y. X.; He, Y. H.; Ran, R.; Weng, D. *In situ* synthesized MoS_2/Ag dots/Ag_3PO_4 Z-scheme photocatalysts with ultrahigh activity for oxygen evolution under visible light irradiation. *Appl. Surf. Sci.* **2018**, *450*, 441–450.

[222] Wei, D. Q.; Ding, Y.; Li, Z. H. Noble-metal-free Z-Scheme MoS_2-CdS/WO_3-MnO_2 nanocomposites for photocatalytic overall water splitting under visible light. *Int. J. Hydrogen Energy* **2020**, *45*, 17320–17328.

[223] Chang, K.; Mei, Z. W.; Wang, T.; Kang, Q., Ouyang, S. X.; Ye, J. H. MoS_2/graphene cocatalyst for efficient photocatalytic H_2 evolution under visible light irradiation. *ACS Nano* **2014**, *8*, 7078–7087.